Triassic stratigraphic evolution of the Arabian-Greater India embayment of the southern Tethys margin

Autor(en): **Hauser, Marc / Martini, Rossana / Burns, Steve**

Objekttyp: **Article**

Zeitschrift: **Eclogae Geologicae Helvetiae**

Band (Jahr): **94 (2001)**

Heft 1

PDF erstellt am: **25.09.2024**

Persistenter Link: https://doi.org/10.5169/seals-168876

0012-9402/01/010029-34 $1.50 + 0.20/0
Birkhäuser Verlag, Basel, 2001

Triassic stratigraphic evolution of the Arabian-Greater India embayment of the southern Tethys margin

MARC HAUSER,[1] ROSSANA MARTINI,[2] STEVE BURNS,[1] PAULIAN DUMITRICA,[3] LEO KRYSTYN,[4] ALBERT MATTER,[1] TJERK PETERS[1] & LOUISETTE ZANINETTI[2]

Key words: Stratigraphy, Sedimentology, Carbon isotope, Oxygen isotope, Triassic Batain Basin, Oman

ABSTRACT

An exceptional, tectonically remarkably unaffected, nearly 200 m-thick continuous section of hemipelagic and turbiditic sediments, covering most of the Triassic is described from the Batain Complex of north-eastern Oman. According to conodont and radiolarian data the sequence spans the late Scythian to the early Norian, a time period of nearly 30 M. Coupled with a high resolution stratigraphy, the lithostratigraphy, sedimentology, as well as sequence and isotope stratigraphy of the section are documented.

For the Triassic of the Batain Plain we propose the new name Sal Formation, which replaces the formerly used Matbat Formation, and subdivide it into three new members. The Sal Formation was deposited on the proximal continental margin of northeastern Arabia and records various depositional environments. The lower member is interpreted as the distal part of a homoclinal ramp which evolves to a distally steepened ramp during time of deposition of the middle member. The upper member displays a toe of slope position which is indicated by an increase of proximal turbidites. These sediments form part of a segment of the Neo-Tethyan embayment between Arabia and India.

The stratigraphic analysis indicates highly varying sedimentation rates from a minimum of 2 m/Mγ around the Anisian/Ladinian boundary up to 15 m/Mγ during the Lower and Upper Triassic. Sequence-stratigraphically, the Sal section is subdivided into six third order cycles which are biochronologically well integrated into the global Triassic cycle chart. The mixed siliciclastic-calcareous upper member of the Sal Formation typically shows highstand related carbonate shedding. It is, therefore, an important test case for sequence-stratigraphic controlled carbonate export to mixed basin fills. The well developed sequence stratigraphic cycles are mirrored in the isotope patterns. Additionally, the carbon and oxygen isotope data from the Sal Formation record the same chemostratigraphic marker at the Spathian/Anisian boundary known from other Tethyan sections.

ZUSAMMENFASSUNG

Eine ungestörte, ca. 200 m mächtige Abfolge aus Turbiditen und hemipelagischen Sedimenten präsentiert einen grossen Teil der Triassedimente des Batain Komplexes des NE-Omans. Das Profil umfasst einen Zeitraum von ca. 30 Millionen Jahren vom Oberen Scythian bis ins Untere Norian und ist mit seiner hoch aufgelösten Conodonten- und Radiolarienbiostratigraphie einzigartig für den südlichen Tethysrand. Basierend auf Biostratigraphie, Lithostratigraphie und Sedimentologie wurde das Profil mit Sequenz- und Isotopenstratigraphie untersucht. Aufgrund der neuen Daten und Erkenntnisse definieren wir ausschliesslich für die Batain Region neu die Sal Formation mit ihren drei Untereinheiten und ersetzen damit die in den Oman Mountains definierte Matbat Formation.

Die Sedimente der Sal Formation wurden in verschiedenen proximalen Ablagerungsräumen in einem Meeresbecken der Neo-Tethys zwischen Arabien und Indien abgelagert. Diejenigen der Sal Formation, die am arabischen Kontinentalrand abgelagert wurden, zeigen zudem einen Wechsel der Beckenarchitektur von einer distalen homoklinalen Rampe zu einer sich vertiefenden Rampe und schliesslich zu einem Beckenabhang mit Turbiditsedimentation. Im Typ-Profil zu sehen sind Meeresspiegelschwankungen und wechselnde Sedimentationsraten der südlichen Tethys, weiter der Zusammenhang zwischen Sequenz- und Isotopenstratigraphie, sowie ein deutlicher chemostratigraphischer Isotopenmarker für die Spathian/Anisian Grenze. Diese Erkenntnisse lassen sich mit Daten des nördlichen Tethysrandes vergleichen und mit globalen Ereignissen in Zusammenhang bringen.

Introduction

The geology of the Batain Plain is dominated by imbricated allochthonous units, consisting of folded and faulted Permian to Late Cretaceous marine sediments and volcanic rocks (Roger et al. 1991; Béchennec et al. 1992b; Wyns et al. 1992) and fragments of ophiolites from the Batain Group (Immenhauser et al. 1998). This Batain nappe stack may reach 1.5-2 km in thickness according to Beauchamp et al. (1995). Because of the relatively scattered outcrops of the different lithologies and apparently chaotic structural situation, they were previously interpreted as "Batain Melange" (Shackleton et al. 1990). Based on lithologic similarities between the Hawasina Basin and the Batain Basin, Glennie et al. (1974),

[1] Corresponding author: Marc Hauser, Mineralogisch-petrographisches Institut und Geologisches Institut, Universität Bern, Baltzerstrasse 1, 3012 Bern, Switzerland. E-mail hauser@mpi.unibe.ch
[2] Département de Géologie et Paléontologie, Université de Genève, 13 rue des Maraîchers, 1211 Genève 4, Switzerland
[3] Institut de Géologie et Paléontologie, BFSH2 UNIL, CH-1015 Lausanne, Switzerland
[4] Institut für Paläontologie der Universität Wien, Althanstrasse 14, 1090 Wien, Austria

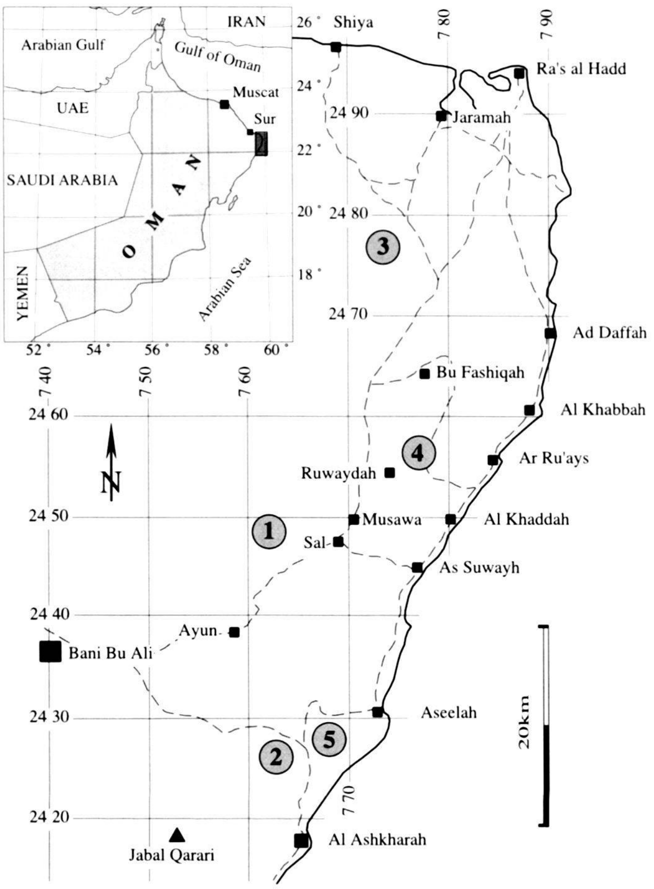

Fig. 1. Simplified topographic map of the Batain Plain with the location of measured lithologic sections discussed in the text.

Roger et al. (1991), Béchennec et al. (1992b) and Wyns et al. (1992) considered the allochthonous sedimentary units of the Batain Plain as a part of the Hawasina nappes (sensu Robertson et al. 1990).

Structural data however, indicate a WNW directed nappe emplacement with NNE-SSW trending folds and thrusts, in contrast to the south to south-west thrusting direction of the Hawasina nappes (Immenhauser et al. 1998; Schreurs & Immenhauser 1999). The WNW oriented obduction is similar to the obduction direction of the Masirah Ophiolite (Marquer et al. 1995). Structural, biostratigraphic and sedimentological data suggest that the obduction of the Batain allochthonous sequence onto the north-eastern Oman continental margin occurred coeval with the obduction of the Masirah Ophiolite, at the Cretaceous/Paleogene boundary (~65 M). This is about 15-20 Mγ later than the SW-directed emplacement of the Semail Ophiolite and the Hawasina Nappes onto the northern continental margin of Oman (Allemann & Peters 1992; Glennie et al. 1974).

This paper deals with the Triassic succession of the Batain Group and summarises the results of extensive field work including mapping at the 1:100'000 scale, logging of sections, as well as microfacies analysis, biostratigraphy, sequence stratigraphy and stable isotope stratigraphy. Based on these data we propose a sedimentary and stratigraphic reconstruction of the proximal north-eastern Triassic Oman margin. Further, we discuss the contrasting evolution of the Batain Basin which was an embayment of the southern Tethys, as compared to that of the Hawasina Basin.

Geological setting

The Batain Plain is located in north-eastern Oman, southeast of the town of Sur (Fig. 1). It extends about 130km northeast-southwest and 40 km east-west and is bounded on the north by the Gulf of Oman and on the east by the Arabian sea. The Wahibah Sands separate the Batain Plain in the west from Interior Oman. Recent sand and gravel deposits cover an extensive part of the area.

The Batain Plain (Fig. 2) comprises the Batain nappes which are composed of Permian to Maastrichtian marine sediments, as well as volcanic rocks and the Eastern Ophiolite nappe. The nappes are unconformably overlain by Autochthonous Late Paleocene to Miocene continental siliciclastic and shallow marine calcareous sediments (Fig. 2). Tectonically, the Batain nappes are characterised by intense folding and thrusting. Outcrops of the Triassic series occur throughout the Batain area and typically form brownish-grey to dark-brown weathering hills. Complete successions with minor tectonic disturbance rarely exceed several tens of meters, except for the section found 6 km WNW of the little village of Sal (Fig. 1) which exposes a succession more than 180 meters thick.

Previous work

Initial geological investigations in Oman were carried out in the early 1960s by the Petroleum Development Oman (PDO) and Shell geologists. The classical study of the Oman Mountains by Glennie et al. (1974) became the basis for much subsequent research. These authors included the Batain sediments in the Late Permian to Early Jurassic Ibra Formation, and the Late Triassic to Early Cretaceous Halfa Formation, both part of the Hawasina allochthonous units (Fig. 3).

In the early 1980s, Amoco Petroleum Company (International) funded a major field-based research program in Oman. In the course of this project (1981–1987), detailed regional correlations were established throughout the Oman Mountains and published as a summary of alternative stratigraphic nomenclature. Bernoulli & Weissert (1987) found that in the central Oman Mountains the Halfa Formation is Late Triassic in age, rather than Late Triassic-Early Cretaceous as proposed by Glennie et al. (1974). They included the Halfa radiolarites in the Al Ayn succession. Bernoulli & Weissert (1987), Cooper (1987, 1990), and Bernoulli et al. (1990) correlated the lower part of the Halfa Formation and the Haliw Formation with the Zulla Formation (sensu Glennie et al. 1974) of the central and northern Oman Mountains. Furthermore, Bernoulli et al.

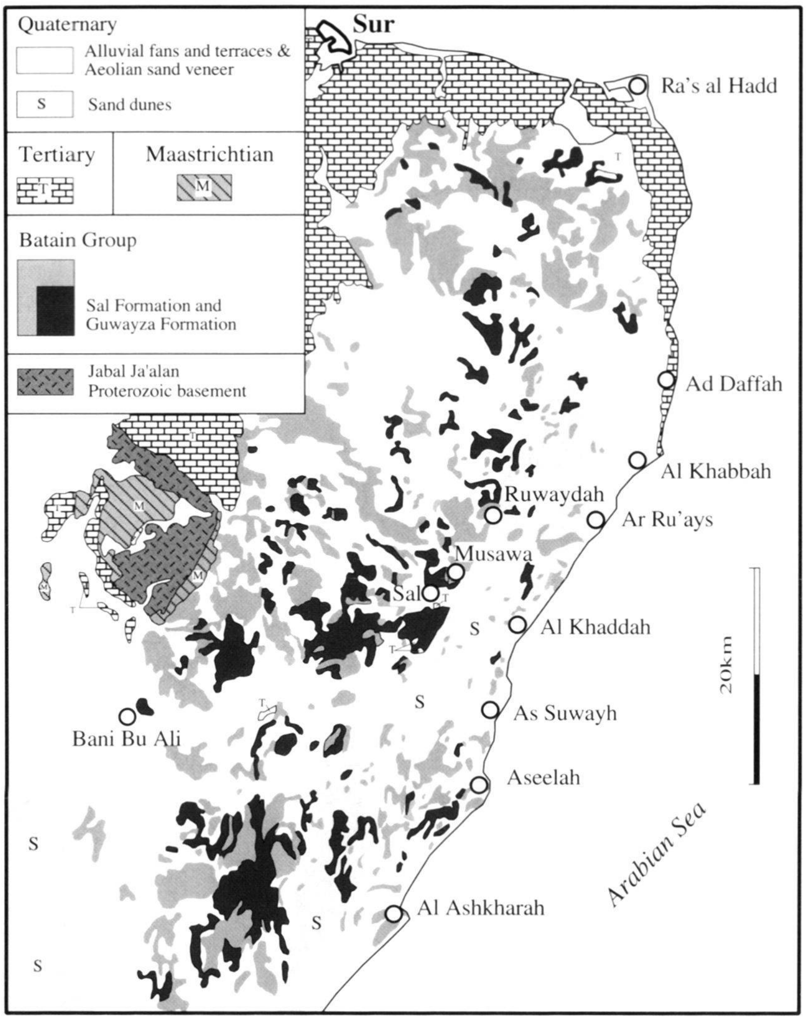

Fig. 2. Simplified geological map of the Batain Plain, showing the outcrop distribution of the Sal Formation and the Guwayza Formation.

(1990) equated the Al Ayn Formation of Glennie et al. (1974) with the Zulla Formation sensu Cooper (1987) and distinguished four new lithological members within the Zulla Formation (Fig. 3).

Between 1982 and 1990, the Bureau de Recherches Géologiques et Minières (BRGM) introduced a new lithostratigraphic nomenclature for Oman, based on their 1:100'000 mapping program in the Central Oman Mountains. Béchennec (1987) replaced the Zulla Formation and the Guwayza Sandstone Formation sensu Cooper (1987) in the Oman Mountains (Fig. 1), with the newly introduced Al Jil and Matbat formations (Fig. 3). During a subsequent mapping program, Béchennec et al. (1992a) redefined the Matbat Formation, in order to include within the lower member a sequence of Carnian radiolarian cherts and shales previously attributed to the upper member of the Al Jil Formation (Fig. 3).

Immenhauser et al. (1998) made an attempt to integrate their divergent biostratigraphic results into the stratigraphic terminology used on the BRGM geological maps. They continued, therefore, to use the formation and unit names introduced by Roger et al. (1991), Béchennec et al. (1992b), and Wyns et al. (1992) for the Batain series, but in a modified sense. Importantly, they recognised significant differences between the Hawasina series and the Batain series and defined the Batain Group for the latter (Fig. 3).

During our subsequent studies in the Batain area we had to solve the problem that lithologically identical rocks were attributed by Wyns et al. (1992) and Béchennec et al. (1992b) partly to the Al Jil Formation and partly to the Matbat Formation. Rather than redefining those formations again we prefer to establish a new formation for certain Triassic rocks of the Batain Plain, for the following reasons: (i) the lack of general lithological and age correspondence with both the Al Jil and the Matbat Formation as defined in the Oman Mountains (Béchennec 1987; Béchennec et al. 1992a) and with the Zulla Formation sensu Glennie et al. (1974) and Bernoulli et al. (1990); (ii) the complete missing of age diagnostic data from the sections known in the Oman Mountains which hampers any detailed correlation with our Batain series; (iii) the Sal section represents a continuous well exposed and well dated se-

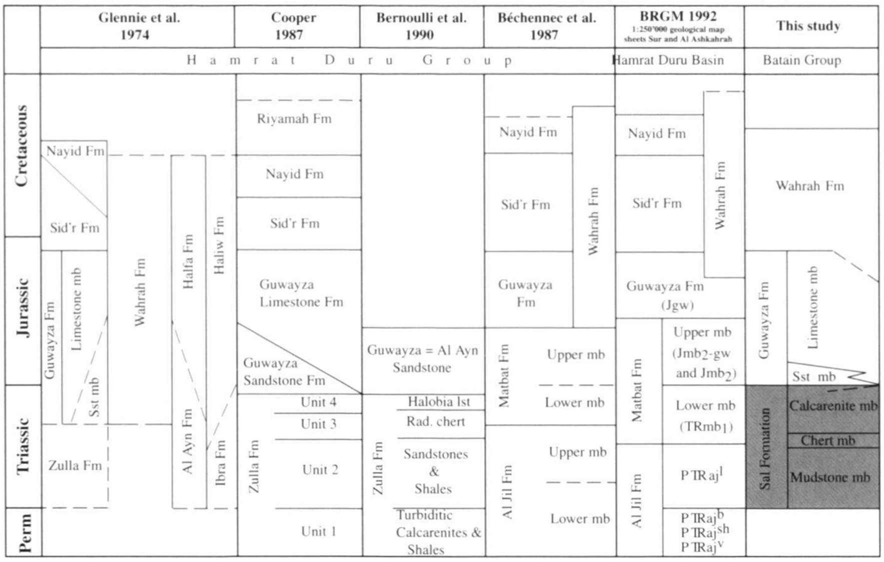

Fig. 3. Relationship between the alternative stratigraphic nomenclature and the different stratigraphic subdivisions for the Hamrat Duru Group and the Batain Group.

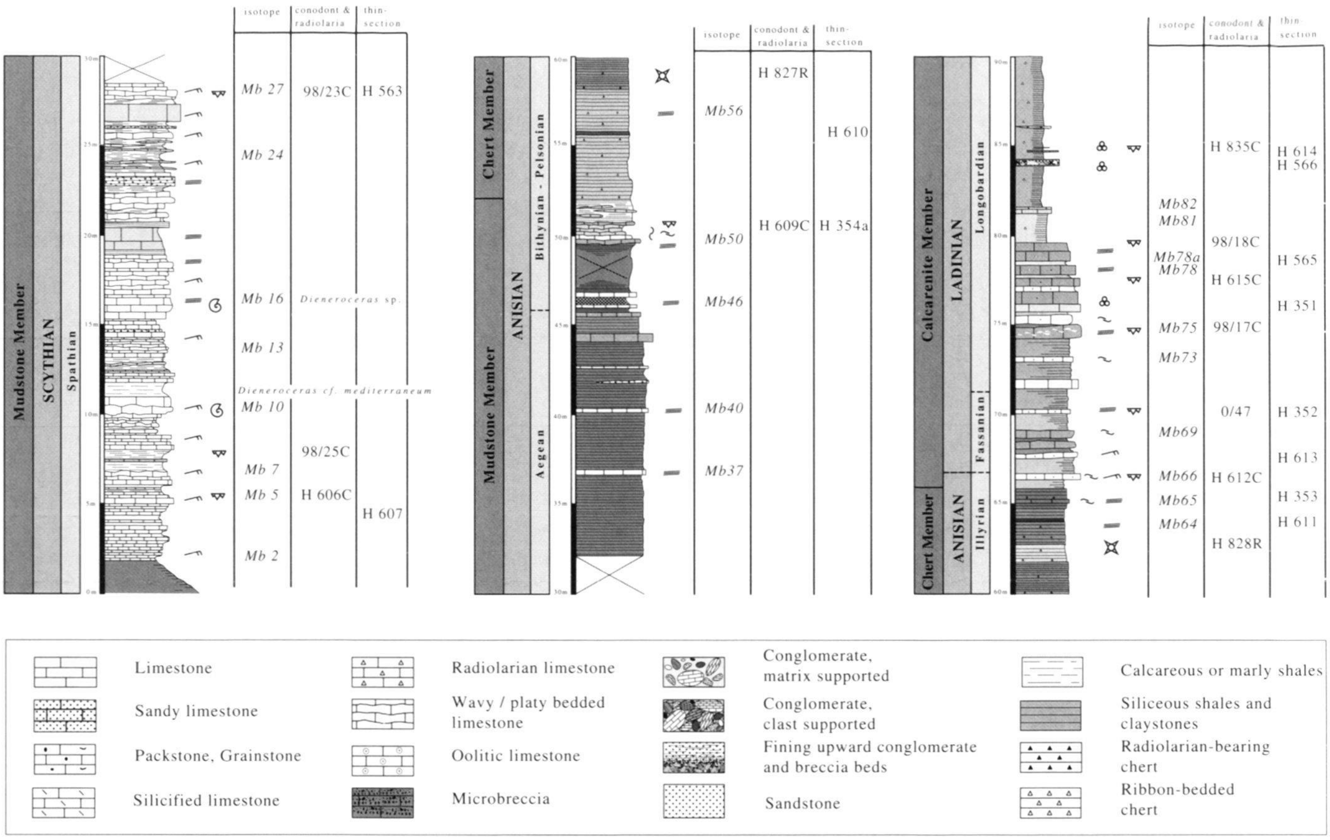

Fig. 4. Lower part of the lithostratigraphic section of the Sal Formation at the locality 1 (762478/2449654) 7 kmWN of the village of Sal.

quence encompassing nearly the entire Triassic. This new formation (Sal Formation) is defined at the locality 7 km WNW of the village Sal (762478/2449654), (Fig. 1, locality 1).

1. Lithostratigraphy of the Sal Formation

The Sal Formation is subdivided from base to top into three mappable members ranging in age from Scythian to Rhaetian (Fig. 3).

Mudstone Member: This 50m thick member consists of grey-brown flaggy limestones, calcilutites and partly silicified pale green to yellowish calcareous shales and claystones. It was considered as the uppermost part of the Al Jil Formation by Roger et al. (1991), Béchennec et al. (1992b), and Wyns et al. (1992).

Chert Member: This is 15m thick and comprises purplish-red and greenish radiolarian cherts with shaly partings, pale green to yellowish claystones and interbeds of strongly silicified radiolarian-bearing limestones.

Calcarenite Member: This member consists of brownish, partly silicified calcarenites with thin-shelled pelagic bivalves (filaments), alternating with radiolarian-bearing cherts and mudstones, and siliceous or limy shales. Isolated calcirudite interbeds are also present. The estimated thickness of this member varies from 115 up to 150 m.

The newly defined Chert – and Calcarenite members are equivalent to units mapped as the lower member of the Matbat Formation (Trmb1) on the sheet 1:100'000 Ja'alan (Roger et al. 1991) and the sheets 1:250'000 of Al Ashkharah (Béchennec et al. 1992b) and Sur (Wyns et al. 1992). Based on lithology and age, we assign their upper Matbat member (Jmb2) and undifferentiated Matbat and Guwayza Formation (Jmb2-gw) to the Guwayza Formation (Fig. 3).

The lower formation boundary of the Sal Formation (Fig. 4) is defined at the type locality at the base of the Mudstone Member, previously considered as the uppermost part of the Al Jil Formation by Roger et al. (1991), Béchennec et al. (1992b) and Wyns et al. (1992). A primary stratigraphic contact between the Mudstone Member and the Al Jil Formation as shown by Béchennec et al. (1992b) is not exposed in the Batain Plain.

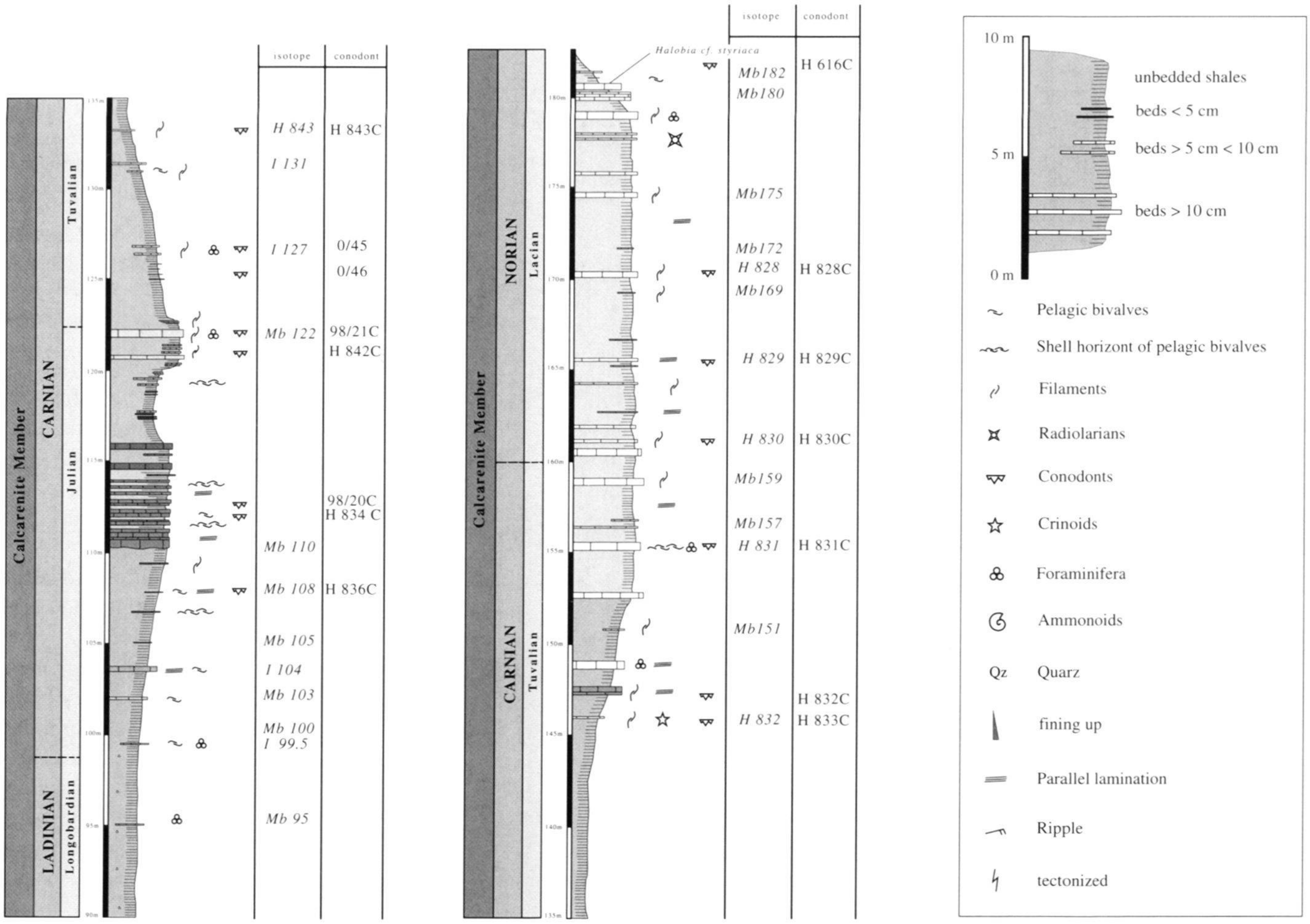

Fig. 5. Upper part of the lithostratigraphic section of the Sal Formation at the locality 1 (762478/2449654) 7kmWN of the village of Sal.

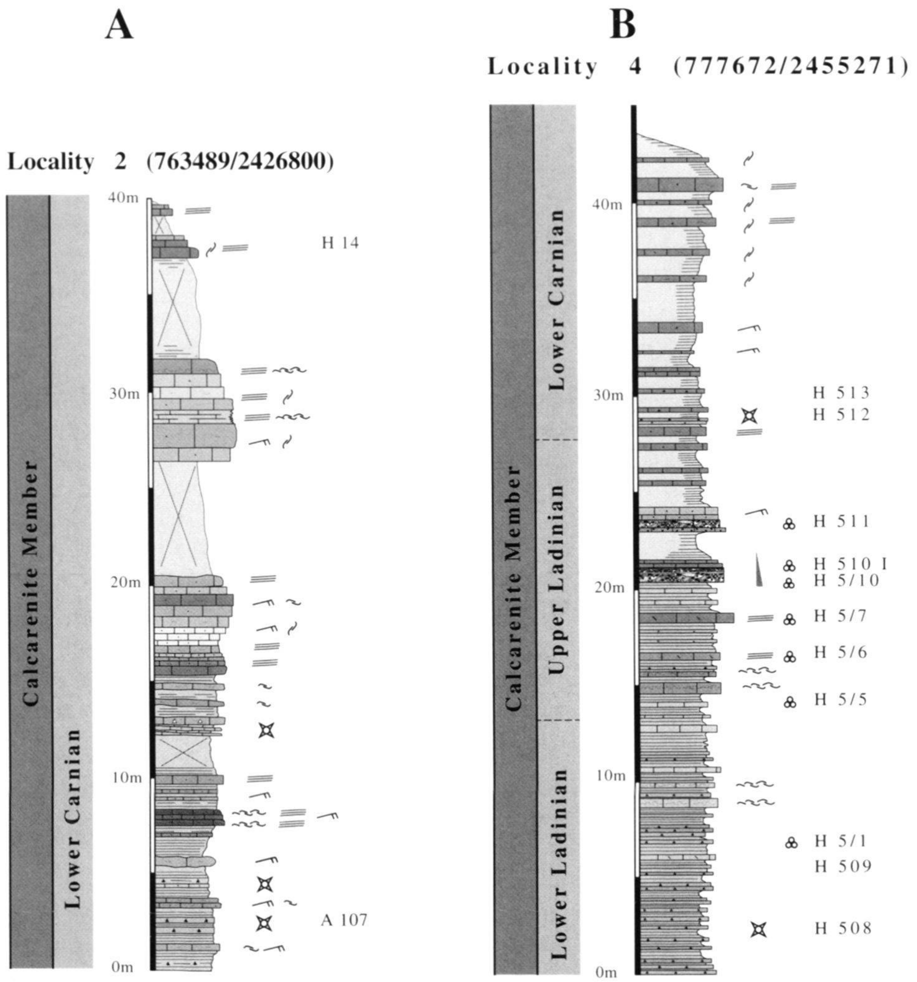

Fig. 6 A. Lithostratigraphy of a part of the calcarenite Member of the Sal Formation dominated by the characteristic filamentous limestones and Early Carnian radiolarian cherts.
B) Detailed section of a part of the Calcarenite Member with Early Ladinian to Early Carnian radiolarian cherts and microbreccia interbeds.

The upper formation boundary is exposed at the locality 3 km SW of Aseelah (769662/2428915) (Fig. 1, locality 2). There, the Calcarenite Member of the Sal Formation is overlain by the Guwayza Formation. The Guwayza Formation is distinguished from the Sal Formation by the presence of calcareous sandstones and oolitic calcarenites devoid of pelagic bivalves.

The composite lithologic section of the Sal Formation ranges from the Spathian to the Rhaetian based mainly on conodonts.

The Mudstone and the Chert Members are well exposed at the type locality (Fig. 4 and Fig. 5). This section shows the contacts between the Mudstone and Chert Members as well as the contact between the Chert and the Calcarenite Members. The Calcarenite Member at the type locality consists mainly of a limestone-dominated facies, whereas in the sections at localities north of Al Ashkahrah (763489/2426800) (Fig. 6A) and northeast of Ruwaydah (777672/2455271) (Fig. 6B) filamentous limestones, radiolarian-bearing cherts and shales are also present.

The Chert and Calcarenite members contain several meter-thick lamprophyre sills, basaltic flows and gabbro intrusions. At a locality 8 km WSW of Sal (760260/2444889), a gabbro intrusion produced a contact aureole in the neighbouring limestones that contains tremolite pseudomorphs.

The Mudstone Member

This lowest member of the Sal Formation is widespread in the middle and southern part of the Batain area. It tends to occur at the foot of the hills built up by the Sal Formation.

At the type locality (Fig. 4), the Mudstone member measures 50 m. The member starts with 30 m of beige-grey platy, wavy-bedded mudstones and very fine-grained calciturbidite, interbedded with yellow-brown calcilutites, marls and calcareous shales. The centimetre-thick turbidites consist of incomplete, base-cut-out Bouma T_c-T_e sequences with erosive basal contacts. The predominant sedimentary structures are ripple cross-lamination, hummocky cross-bedding and in some beds a millimetre to centimetre-scale planar lamination. Sole marks are rare, but isolated flute casts were recognised.

The flaggy limestones are conformably overlain by less than 20 m of thin-bedded pale-green claystones and silty shales with intercalations of centimetre-thick beds of grey-brown mudstones and rare sandy limestones (Fig. 4). The Mudstone member ends with a one metre thick horizon of nodular, thin-bedded and weakly laminated limestones, containing rare layers of thin-shelled bivalve filaments. In some of these beds a weak bioturbation is observed. At the surfaces of some of the nodular limestone beds ferrugineous crusts and millimetre-sized nodules occur.

Microfacies and age

The dominant microfacies of the limestones is a homogeneous, sometimes thinly laminated, mudstone (microsparite) containing millimetre thick coquinas of ostracods and conodonts. The thinner bedded and rippled calciturbidites are made up of bioclastic packstones and grainstones with worn bioclastic grains, calcite-replaced radiolarians, small ostracods, echinoderms, rare benthic foraminifers (Nodosariidae) and peloids.

The lower part of the Mudstone member has been dated as Lower Triassic (Spathian) on the basis of two ammonoid horizons with *Dieneroceras* cf. *mediterraneum* and the conodont assemblage (H606, 98/25, 98/23) (Tab. 1), whereas the top of the Mudstone member is of Middle Anisian (Bithynian) age, dated by conodonts (H609C), (Tab. 1).

The Chert Member

The 15 m thick Chert member is made up of 1 to 10 cm thick, regularly bedded pale green to yellowish claystones, purple and copper-green radiolarian cherts with shaly partings and interbeds of strongly silicified radiolarian-bearing limestones.

At locality 6 km WNW of Sal (Fig. 1), one single 2-3 cm thick tuff layer was found within the Chert member, whereas about 5 km SE of Ayun (761047/2435522), 1m thick lapilli-bearing tuff is present within approximately 15 m of radiolarian cherts.

Microfacies and age

The microfacies of the Chert Member is composed of radiolarian cherts and radiolarian packstones, silicified grainstones with echinoderm fragments, filaments of pelagic bivalves and rare Nodosariidae. The clay-rich siliceous matrix of the mud and packstones contains abundant radiolarian moulds.

The radiolarian fauna of the Chert member is of Late Anisian age (H827, H828) (Table 2).

The Calcarenite Member

The radiolarian cherts of the Chert Member gradually pass upward into a carbonate-bearing succession of the Calcarenite Member, whose estimated thickness is at least 100 m (Fig. 4 and Fig. 5). The lower 15 m of the Calcarenite Member consist of mainly 10 to 40 cm thick beds of brownish calcarenite, greenish shaly marls and radiolarian-bearing mudstones and cherts. They are overlain by more than 20 m of siliceous shales and cherts without well developed limestone beds. The shales gradually pass upwards into a sequence of alternating siliceous shales, radiolarian micrite, calcarenite and filamentous limestones.

The limestone beds show a brown to black patina. In places they are silicified and consist of planar laminated calcarenite and of incomplete Bouma T_b-T_e turbidites. The laminated calcarenite and the filamentous limestones are characterised by the presence of centimetre-thick layers of thin-shelled pelagic bivalves of the *Halobia-Daonella* type. At the type locality (Fig. 4 and Fig. 5) and NE of Ruwaydah (777672/2455271) (Fig. 6B), the Calcarenite Member contains interbeds of polymict calcirudite that are a few to 20 cm thick.

At locality 6, 3 km SW of Aseelah (Fig. 1) the uppermost 60 m of the Calcarenite Member contain a centimetre to decimetre thick, poorly bedded calcarenite-calcsiltite-shale succession. The beds show a thinning-up trend, plane lamination, ripples and isolated slump structures. The quartz content in the limestones and the proportion of shales increases up-section. The Calcarenite Member grades conformably upward into the overlaying Guwayza Formation.

The predominant sedimentary structures within the Calcarenite Member are millimetre thick parallel laminations and swaley cross-stratification similar to hummocky cross-stratification. Weakly fining- and thinning-upward sequences were also found within the calcarenites. The cross-stratification is characterised by low amplitude ripples (1 to 3 cm) undulating as a series of broad anticlines and synclines. The ripples are made up of wispy indistinct laminae which frequently thicken in the anticlines and pinch-out in the synclines or pass laterally into plane laminations.

Microfacies and age

The microfacies of the Calcarenite Member consists of planar laminated limestones, and thin bioclastic grainstones and packstones (biopelmicrosparite to sparite), which yield masses of oriented thin-shelled valves of *Halobia-Daonella* type, together with recrystallised radiolarians, abundant foraminifera (Nodosariidae) and micritic peloids (see Glennie et al. 1974; Shackleton et al. 1990; Béchennec et al. 1992b). The radiolarians are often strongly recrystallised and not identifiable.

The cross-stratified T_c turbidite beds, made up of weakly graded grainstones and packstones with wackestone tops (calcarenites), consist of reworked fine-grained litho- and bioclasts, deposited within distinct lenticular layers. These layers are often separated by millimetre-thick laminated lime mud. The carbonate detritus consists of small, worn bioclastic grains, peloids, and rare ooids. The bioclasts include benthic foraminifera (Tab. 3), ostracods, gastropods, and remnants of echinoderms and algae. These shallow-water elements in the detritus were derived from a shallow carbonate ramp environment. A well preserved autochthonous population of conodonts (Pl. 1) and filaments were also observed in thin section. They are associated with allochthonous conodonts, reworked from the proximal basin floor during their transport into the distal part of the basin.

Unsorted polymict calcirudite interbeds are composed of angular to rounded, millimetre- to several centimetre-sized clasts and boulders, supported by a sparite cement. The clasts are made up of reworked carbonate litho- and bioclasts, volcanic clasts and chert fragments. Identifiable fossils include foraminifera, small gastropods, ostracods, remnants of algae and echinoderms; coral fragments and embryos of ammonites. The calcirudite also contains Permian bioclasts, with fragments of Fusulinids and Bryozoans.

The conodont, radiolarian, and foraminiferal assemblages (Tab. 1–3) indicate a Ladinian to Rhaetian age for the Calcarenite Member.

2. Biostratigraphy

Conodonts

The Sal Formation contains abundant conodonts with a low CAI index of 1 in the Mudstone and Calcarenite members. The Chert Member may contain conodonts but was not sampled due to the absence of limestone intercalations.

Conodonts from the Mudstone Member are well preserved, relatively small and dominated by specimens of the genus *Neospathodus*. They are completely preserved, including the delicate ends of the teeth, and are therefore interpreted as autochthonous, although transport by mud turbidites or distal tempestites within a soft matrix can not be excluded. Within the Calcarenite Member, only the filament-and radiolarian-bearing wackestones (e.g. H834, H842, H832) contain autochthonous conodonts. All sampled calcarenites (pack- and grainstones) contain conodonts of highly varying ages including even Permian species (Tab. 1). These samples are rich in large platform conodonts which are often fragmented and only rarely well preserved. The age determination of the calcarenite samples was based on the youngest occurring conodonts which are usually much more common than reworked ones. The age range of reworked conodonts increases up-section, documenting increasing erosion and redeposition of intrabasinal sediment. The reworked conodont fauna is composed of Permian (Roadian-Wordian) gondolellids, Early Triassic neospathodids and Middle to Late Triassic *Neogondolella*, *Gladigondolella*, *Metapolygnathus* and *Epigondolella* species. Records of Late Permian and lowermost Triassic conodonts are completely missing and it may be that sediments of this age were either not deposited or were removed prior to the deposition of the Sal Formation. Redeposition of Permian sediments near the Permian/Triassic boundary may be a distinct feature of proximal basin parts of the Oman allochthon (e.g. Wadi Wasit area – Blendinger 1988).

Biochronological dating of the samples is based on conodont-ammonoid calibration schemes by Orchard (1995) for the Early Triassic, Nicora (1977) and Krystyn in Gallet et al. (1998) for the Middle Triassic and Krystyn (1980) as well as Krystyn in Gallet et al. (1994) for the Late Triassic. The base of the section (H606) and the overlaying calcareous part of the Mudstone Member (98/23, 98/25) are dated by *N. cf. homeri* (Pl. 1, Fig. 5), *N. symmetricus* and *N.* cf. *abruptus* (Pl. 1, Fig. 8) as Spathian, 98/25 also yields *N. cf. jubata*. The next fossiliferous sample H609 from 20m above contains *N.* cf. *regularis*, a distinct Anisian (Bithynian) form. No conodonts are known from the shaly interval in between which, according to its position, is tentatively attributed to the Early Anisian (Aegean). Conodonts are also missing from the 15m succession of radiolarian cherts dated indirectly by the faunas below H609 and above H612 (Fig. 4B, C). The succeeding limestone-shale sequence of the Calcarenite Member contains *N.* cf. *praeszaboi* at its base (H612) which is thought to represent the basal Illyrian. Just 3m above, sample (0/47) contains *P. excelsa*, *N. transita* and *B.* cf. *hungaricus* recording a Late Fassanian age. Four metres above (98/17), *P. inclinata*, *P. trammeri* (Pl. 1, Figs. 9, 15) and *B. hungaricus* occur, recording an early Late Ladinian (Longobardian) age. The topmost Anisian and Early Ladinian are, therefore, very condensed. An early Late Ladinian age is further indicated in H615 by the presence of *B. japonicus*. Samples 98/18 and H835 contain *P. inclinata* and *B. mungoensis* (Pl. 1, Figs. 2, 14) and are thus of Middle to Late Longobardian age. Between H835 and the first Carnian sample H836, more than 20 m of undated siliceous shales without well developed limestone beds are present. Consequently, we have interpolated the Ladinian/Carnian boundary halfway in between. This procedure is strengthened by the age of sample H836 which is placed stratigraphically well above the boundary as it contains *M. carnicus* (Pl. 1, Fig. 11), a species diagnostic for the middle part of the Early Carnian (Gallet et al. 1994). The other Early Carnian samples H836, H834, 98/20, H842 and 98/21 are marked by *Gladigondolella*, *M. polygnathiformis* (Pl. 1, Fig. 13) and *M. foliatus*, sample H842 also contains *M. auriformis* (Pl. 1, Fig. 12).

The Lower/Upper Carnian boundary is drawn directly above 98/21 since sample 0/46 located 3 m higher up yielded a rich and exclusive *Metapolygnatus* fauna composed of *M. polygnathiformis* and subordinate *M. carpathicus* (Pl. 1, Fig. 6). The latter is a distinct guide for the Middle Tuvalian, hence a hiatus may exist in the basal Tuvalian. A Middle Tuvalian age is further indicated by samples 0/45 and H843. The succeeding 20 m thick uppermost Carnian (Tuvalian 3) and 25 m thick lowermost Norian (Lacian 1) intervals are best documented by conodont faunas. Sample H833 still contains *M. polygnathiformis* (Pl. 1, Fig. 13) and *M. nodosus* (Pl. 1, Fig. 10), whereas H832 and H831 are latest Tuvalian as demonstrated by the presence of *M. oertlii* and *M. communisti* A-type sensu Krystyn (1980) (Pl. 1, Fig. 7). The base of the Norian is marked in sample H 830 by the appearance of *N. navicula* (Pl. 1, Fig. 1), which is also present section upward in samples H829 and H828. Still earliest Norian is recorded in sample H616 by *E. quadrata*, a date in accordance with the co-occurring *Halobia* cf. *styriaca*, a pelagic bivalve guide for the Lacian 1.

Although younger Norian rocks are missing in the Sal section, the same lithology seems to have continued towards the

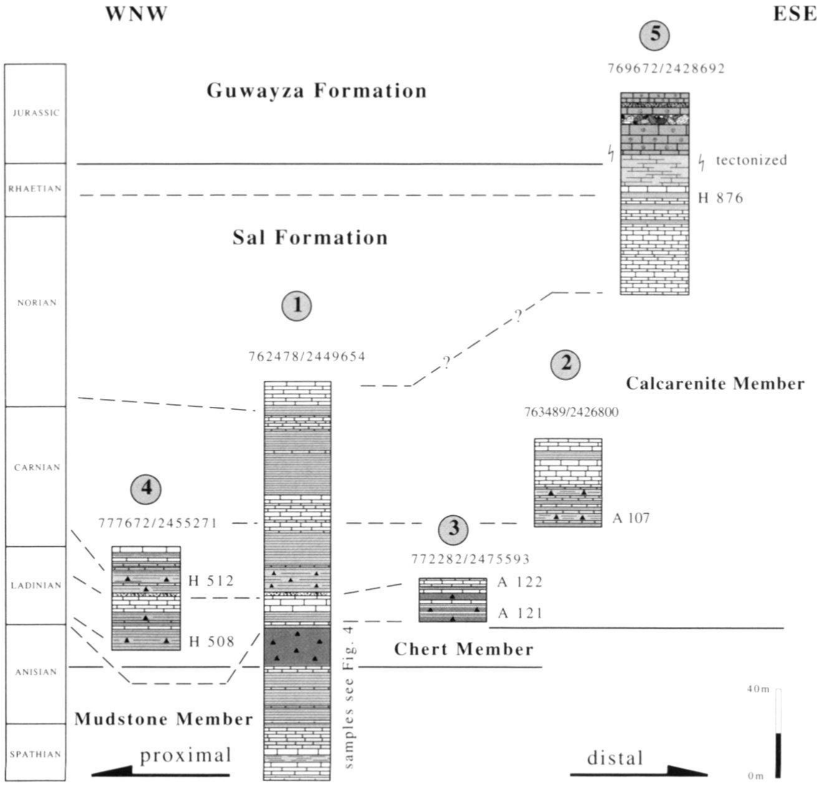

Fig. 7. Triassic stratigraphy and facies variations of the Sal Formation in the Batain Plain showing an increase of radiolarian cherts from proximal to distal parts of the basin.

top of the Triassic as documented in another outcrop (section 6 in figure 7). Here, an early Rhaetian fauna consisting of *M. hernsteini* and *M. posthernsteini* is present accompanied by reworked Permian and Norian conodonts. Reworked conodonts are represented in the Sal section from the Ladinian onwards. The samples H830 and H831 contain Permian (Pl. 1, Fig. 3) as well as Early Triassic (Pl. 1, Fig. 4), Middle and lower Late Triassic forms. Sample H835 yields Permian to Middle Triassic reworked forms, samples 98/17, H836, and H828 Permian and Early Triassic reworked conodonts. Sample 98/21 contains only Lower Triassic reworked conodonts whereas H615 Middle Triassic displays reworked forms. Samples 98/18 and H842 contain only Permian forms.

Radiolarians

Radiolarians of the Sal Formation cover a stratigraphic interval from Late Anisian to Middle Norian (Tab. 2). Their occurrence corresponds to the levels of radiolarian cherts of the Chert and the Calcarenite Members. The preservation varies from very poor to moderate and the number of species determined is usually small. Fortunately, many diagnostic species with fragile tests have robust spines resistant to dissolution which allows species determination. In order to establish the age of radiolarian assemblages we used especially the zonation schemes established by Kozur & Mostler (1994) for the Late Anisian – Early Norian interval, and by Blome (1984) for the Early – Middle Norian.

The Late Anisian-Early Longobardian interval can be recognised and subdivided by the representatives of the family Oertlispongidae, whose evolution and radiation took place particularly within this interval (Dumitrica 1982; Kozur & Mostler 1994, 1996; Lahm 1984, etc.). This family, characterised by the presence of a highly differentiated polar spine, is one of the most important radiolarian families for the stratigraphy of the Tethyan Ladinian and for determination of the Anisian/Ladinian boundary (Kozur 1996). The advantage of using this group of radiolarians is that the diagnostic polar spines are very resistant to dissolution and are preserved even in the poorest preserved faunas.

The oldest radiolarian assemblage of the Sal Formation was found in the section at the type locality (Fig. 4) (H827) (Pl. 2, Figs. 1–2) and is considered Late Anisian in age. It is very poorly preserved, represented by some specimens of *Eptingium manfredi, Pararchaeospongoprunum* cf. *hermi*, and especially by spines of oertlispongids with widened distal part. These spines were assigned to *Paroertlispongus multispinosus* whose first appearance is recorded in the Late Anisian *Paraceratites trinodosus* Zone (Kozur 1996). Although this type of spine ranges up to the Late Fassanian, the absence of spines with a curved distal part assignable to *Oertlispongus* indicates a stratigraphic level below the Anisian-Ladinian boundary.

The Early Ladinian (Fassanian) radiolarian fauna from Oman is roughly similar to that of the Buchenstein Formation, but due to poor preservation a very small number of species characteristic of the latter could be determinated. The oldest Fassanian fauna was also found at the type locality (Fig. 4), in sample H828 (Pl. 2, Figs. 3–14). This fauna too is rather poorly preserved, but it already contains spines of oertlispongids with curved spines assignable to *Pseudoertlispongus mostleri*, considered by Kozur (1996) as the transitional form between *Pseudoertlispongus* and *Oertlispongus*. The absence of any species of the latter genus, known to appear at the base of the Ladinian, suggests, however, that this level is still in the latest Anisian or near the Anisian/Ladinian boundary. The most characteristic and diverse Fassanian assemblage was found in samples P373 and A181. They contain spines of *Oertlispongus inaequispinosus*, *Baumgartneria*, *Falcispongus*, and many other species common in the Fassanian (Tab. 2).

In the Longobardian two assemblages have been recognised: an older one with *Falcispongus hamatus* and *Silicarmiger latus*, but without *Muelleritortis* (A119, Tab. 2) (Pl. 3, Figs. 9–19) and a younger one with *Muelleritortis cochleata*. The former assemblage seems to correspond to the early Longobardian whereas the latter can be assigned to the *M. cochleata* Zone, considered by Kozur & Mostler (1994) to represent the interval between the middle Longobardian and the Ladinian/Carnian boundary. This latter assemblage, characterised by the occurrence of M. *cochleata* against *Tritortis kretaensis*, is common in the Late Ladinian of Oman (H429, A137, Tab. 2).

The Early Carnian levels are characterised by the predominant occurrence of *Tritortis kretaensis* over *M. cochleata* (A107, A137, Tab. 2). According to Kozur & Mostler (1994) this predominance is characteristic of the *T. kretaensis* Zone, which practically corresponds to the Cordevolian. A sample considered as coming from the boundary between this zone and the previous one, (P378, Tab. 2, Pl. 3, Figs. 20–38; Pl. 4, Figs. 1–2) still shows frequent specimens of *Muelleritortis cochleata* in an assemblage within which *T. kretaensis* predominates.

The subdivision of the Middle Carnian (Julian)-Early Norian interval, and the recognition of the Carnian/Norian boundary in Oman is difficult to define on the basis of radiolarians because of the absence of a well established zonation of this interval. In agreement with data by Kozur & Mostler (1994) and Blome (1984) we considered the assemblages containing species of *Capnuchosphaera* without *Capnodoce* as Middle-Late Carnian- ?Early Norian (H844, A198, A56 (Tab. 2) (Pl. 4, Figs. 3–35; Pl. 5, Figs. 1–12). These assemblages also contain *Xiphotheca karpenissionensis*, *Spongostylus* cf. *carnicus*, *Trialatus megacornutus*, *Poulpus piabyx*, and many indeterminable species. The saturnalids are practically absent from this interval in the samples from the Batain Plain .

The Early Norian was established on the basis of the presence of species of *Capnodoce* (A125, Tab. 2) (Pl. 5, Figs. 13–29). This pantanelliid genus is very rare and is usually associated with species of *Capnuchosphaera* whose tubular spines are resistant to dissolution and easily determinable.

The Early? -Middle Norian was identified on the basis of the presence of *Canoptum sp.*, *Corum regium*, *Latium* cf. *paucum* (H621, Tab. 2) (Pl. 5, Figs. 30–35). According to Blome (1984), *Latium paucum* first appears in the upper part of the *Capnodoce* Zone comprising the Early to Middle Norian interval.

No radiolarian assemblage from the Sal Formation contains radiolarians of Late Norian, Rhaetian or Early Jurassic age.

Foraminifera

Benthonic foraminifers, mainly of shallow water origin, occur in the calcarenitic and calciruditic intervals of the hemipelagic Calcarenite Member. Some variations in frequency are observed, which seem to be related to the amount of fine-grained material derived from a carbonate platform. The foraminiferal tests are generally well preserved, except for the hyaline specimens Aulotortidae and Triadodiscidae. The biloculine porcelaneous forms of Meandrospiridae (Turriglomininae) are normally well preserved.

The age diagnostic foraminifers in the calcarenites are (Pl. 6, 7): *Turriglomina mesotriasica* (Koehn-Zaninetti), *T. conica* (He Yan), *Turriglomina* aff. *T. scandonei* Zaninetti et al., *Aulotortus sinuosus* Weynschenk, *A. praegaschei* (Koehn-Zaninetti), *Palaeolituonella meridionalis* (Luperto) and *Triadodiscus eomesozoicus* (Piller).

In the calcirudite, the stratigraphically significant foraminifers are (Pl. 6, 7): *Turriglomina mesotriasica* (Koehn-Zaninetti), *Turriglomina* aff. *T. magna* (Urosevic), *Gsollbergella spiroloculiformis* (Oraveczne-Scheffer), *Aulotortus sinuosus* Weynschenk, *Auloconus permodiscoides* (Oberhauser), *Pilammina gemerica* (Salaj), *Palaeolituonella meridionalis* (Luperto), *Cucurbita* sp., and *Orthotrinacria* sp. (Tab. 3).

In all fossiliferous samples of the Calcarenite Member, additional foraminifers belonging to the families Ophthalmidiidae, Endotebidae, Endotriadidae, Duostominidae and Nodosaridae are also recorded.

The small species *Turriglomina mesotriasica* (Pl. 6, Figs. 8–9, 14–16) and *Turriglomina conica*, (Pl. 6, Fig. 18) characteristic of the basinal environment of the Tethys realm, are the only autochthonous foraminifers in the Calcarenite Member. Indeed, as already shown by Zaninetti et al. (1990), *T. mesotriasica* and *T. conica* occur in hemipelagic facies, in association with conodonts, radiolarians and thin-shelled pelagic bivalves (filaments). In contrast, the larger forms *T. magna* (Pl. 6, Figs. 3–7) and *T. scandonei* (Pl. 6, Figs. 1–2) are allochthonous in deep sea environments. In the Calcarenite Member, they are resedimented from a carbonate platform into the basin as were most other species (except *T. mesotriasica* and *T. conica,* Tab. 3).

The foraminiferal assemblage from the Sal section indicates a time span from the Middle Triassic (Middle Ladinian) to the Late Triassic. The corresponding ranges for the

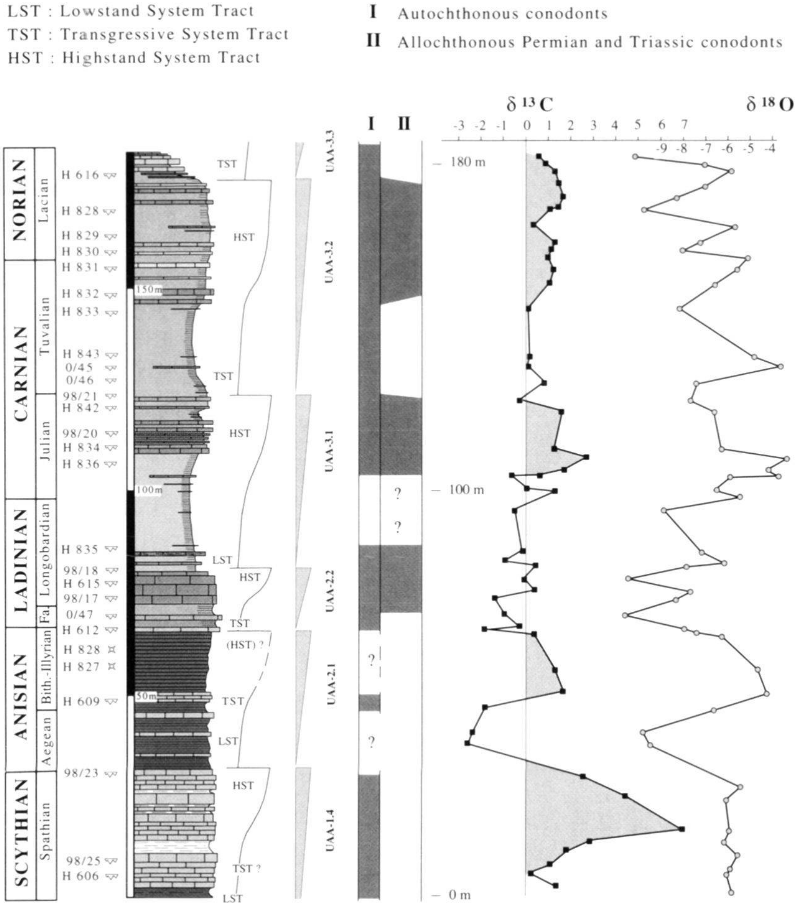

Fig. 8. Combined chrono- litho- sequence- and isotope stratigraphy of the Sal Formation, WNW of the village of Sal. (Geological time scale after Gradstein et al. 1994).

foraminiferal associations are given in (Tab. 3). Concerning the Turriglomininae, their time ranges (Anisian to Ladinian for *T. conica*, *T. mesotriasica*, *T. scandonei;* Anisian to Norian for *T. magna*) are in agreement with those given by Urosevic (1988) for similar microfaunas, also associated with conodonts, from the Carpatho-Balkanides (Eastern Serbia).

3. Carbon and Oxygen Isotopes

Samples for stable isotope analysis were collected at the most complete section measured at the locality 7 km WNW of Sal (Fig. 1, locality 1). This section, more than 180 m thick, is only weakly deformed. The detailed conodont, radiolaria and foraminifera biostratigraphy, carbonate sedimentology and microfacies data allows the isotope results to be placed in a firm stratigraphical context.

Methods and sampling

Carbon and oxygen isotope analyses were performed using standard techniques in the isotope laboratory of the Geological Institute at the University of Berne. For all samples, approximately 10 mg of powdered material was reacted in "100%" H_3PO_4 at 90°C (McCrea 1950) in an on-line automated preparation system. The resulting CO_2 was analysed on a VG Prism II ratio mass spectrometer. Repeated analyses of standard material show a reproducibility of better than 0.1‰ for $\delta^{18}O$ and less than 0.05‰ for $\delta^{13}C$. All results are presented relative to the PDB standard. Thin section examination eliminated samples that had suffered coarse or extensive recrystallisation. To minimise diagenetic influences only micritic whole rock samples were used. The results of stable isotope analyses are given in Table 4.

Description

Within the calcareous base of the section, a well marked positive excursion of $\delta^{13}C$ values was found at the top of the Spathian (Fig. 8), with $\delta^{13}C$ values reaching a maximum of +7‰. The age of this positive excursion is constrained by the conodont fauna (Tab. 1). A rapid decrease of the $\delta^{13}C$ values to as low as –2.57‰ is found in the overlaying siliceous shales of Early Anisian age. A second positive excursion with values up to +1.68‰ occurs in the Bithynian.

The carbon isotope ratios show a gradual increase from negative (–1.64‰) to positive (+0.4‰) values during the Ladinian. This period is characterised by alternating sedimentation of hemipelagic limestones, shales and calciturbidites. In the Early Carnian the $\delta^{13}C$ ratio rise to a maximum value of 2.7‰. The remaining Carnian and Norian are characterised by relatively constant positive values.

A long-term isotopic trend can be observed within the $\delta^{13}C$ pattern. After the strong $\delta^{13}C$ fluctuations in the basal part of the section (Late Scythian and Anisian) a gradual rise of the $\delta^{13}C$ values (app.. 3.5‰) is present for the remainder of the Triassic.

4. Discussion

Depositional environments

The Mudstone Member is dominated by the presence of calcilutites and mudstones, interbedded with flaggy limestones, shales and claystones. Based on the internal organisation of the beds with Bouma T_c-T_e cycles and the presence of hummocky cross-bedding, these deposits are interpreted as tempestites or low-density turbidites, originating from a shallow ramp environment as indicated by the absence of reef-derived debris or base-of slope breccias. Further, the presence of calciturbidite, hemipelagic mudstones with limy shale interbeds containing open marine conodonts indicates a homoclinal distal ramp environment below the fairweather wave base (Read 1982). A low ramp inclination, common for homoclinal ramps (Schlager 1997), a high carbonate content, the absence of radiolarian cherts and the occurrence of tempestites suggest a water depth of less than 200 m. A relatively high sediment accumulation rate of 14 m/Mγ was calculated for the Spathian.

The Chert Member is characterised by claystones, silty shales and radiolarian cherts with rare tuff interbeds. A few siliciclastic limestone intercalations occur within the clay- and siltstones. The sediment accumulation rate decreased from 5.5 m/Mγ during the Anisian to reach a minimum of about 1 m/Mγ in the Illyrian-Fassanian interval. The radiolarian-rich, carbonate-free sediments are probably the result of a deepening of the basin and a rise in the CCD (Cooper 1990). These findings indicate a change of the environmental conditions and were probably favoured by a change of the basin geometry from a homoclinal to a distally-steepened ramp morphology (Read 1982).

The strong decrease of the accumulation rate down to 1 m/Mγ in the Chert member may be seen as a response to a drastic Tethyan-wide sea level rise during the Illyrian-Fassanian time interval. The sediment accumulation rate increased in the Longobardian and Julian to 7 m/Mγ and reached with 15 m/Mγ during the Tuvalian and lowermost Norian the same high values of the Lower Triassic. The accumulation rate of the Calcarenite member increases primarily through the additional input of abundant calciturbidites. They consist of slope-eroded intrabasinal rock fragments as indicated by reworked Permian and Triassic microfossil assemblages (Fig. 8). The complete absence of reef-building organisms (e.g. corals, stromatoporids, calcareous sponges), as well as the common presence of carbonate particles from different shallow-marine environments e.g. ooids, oncoids, echinoderms and dasycladaceans, exclude a carbonate platform rimmed with reefs at the western margin of the proximal Batain Basin. Rather, these observations indicate a ramp-type shelf with a barrierless slope. As a result, towards the distal parts of the basin calciturbidites become less abundant and are replaced by siliceous shales and radiolarian cherts (Fig. 7). The change from the Chert Member to the overlaying Calcarenite Member with its abundant calciturbidites suggests that from the Ladinian to the Early Norian the margin evolved from a distally steepened ramp to a deeper slope and by-pass margin.

Sequence stratigraphy

The type-section of the Sal Formation is a key place for the sequence stratigraphic analysis of a mixed carbonate-siliciclastic system within the Tethyan Triassic. The good biostratigraphic control enables a comparison and correlation with Triassic sequences from other Tethyan margins (De Zanche et al. 1993; Garzanti et al. 1995). The sequence stratigraphic record of the section suggests a direct interplay between sea level changes and the isotope stratigraphy.

The Sal type-section can be subdivided into three second order supercycles with six third order cycles (UAA-1.4, UAA-2.1–2, UAA-3.1–3) following Vail et al. (1991). These cycles (Fig. 8) are dated by conodonts and fit into the Triassic cycle chart of Haq et al. (1988). Hence, no attempt has been made for a local nomenclature (Gionolla & Jacquin 1998).

The Lowstand Systems Tracts (LST) are commonly documented by coarse-grained clastic deposits; breccias, siltstones or calcarenite. In the Sal section, three LST were determined. The shales and mudstones at the base of the section are interpreted as lowstand deposits corresponding to the base of the global UAA-1.4 cycle. The next LST deposits above consist of siltstones and calcarenite interbeds which date the onset of the UAA-2.1 cycle sensu Vail et al. (1991). The last distinct LST is made up of shales with microbreccia interbeds and is used to date the base of the UAA-3 supercycle. The widespread missing of LST deposits in the Calcarenite member may reflect an increasing far-shore position during deposition.

The sediments deposited during Transgressive Systems Tracts (TST) are alternating terrigenous shales and thin-bedded often siliceous limestones which are characterised by an autochthonous microfauna (Fig. 8). Rare thin intervals of pure pelagic filament- and radiolarian-bearing wackestones may be interpreted as local flooding surfaces. Haq et al. (1991) postulate carbonate sedimentation in both the LST and the High Stand Systems Tracts (HST). In the Sal section, the major carbonate accumulation is restricted exclusively to the highstands which is consistent with the model of Schlager et al. (1994). The HST deposits within the Sal section are generally developed as thickening-upward limestone sequences, with the exception of the UAA-2.1 cycle which consists of radiolarian cherts (Fig. 8). The HST deposits of the UAA-2.2, UAA-3.1 and UAA-3.2 consist of calciturbidites with reworked litho- and bioclasts of Permian and Triassic age. They have been deposited at a toe of slope position. Slope erosion normally characterises lowstand phases, but within the Calcarenite Member, seafloor erosion is also common during highstands and not only restricted to lowstands. High carbonate productivity on the shallow shelf coupled with a low subsidence rate and/or oversteeping of the slope (Schlager & Camber 1986) may the prime cause for erosion of the Batain shelf during highstands. The interpretation of radiolarian cherts as HST of the UAA-2.1 cycle can be explained with a profound deepening of the basin and/or a sea level rise contemporaneous with a change from a homoclinal ramp to a distally steepened ramp or slope sensu Schlager (1997).

The shales, mudstones and calcsiltite of Spathian age at the base of the Sal section and the UAA-1.4 cycle (Fig. 4) are comparable with successions known from the Himalayas (Garzanti et al. 1995) and the western Tethys. These calcareous sediments probably indicate the first pulse of higher carbonate production after the Permo/Triassic crisis.

The Anisian is represented by the UAA-2.1 cycle which begins in the early Anisian and ends in the late Anisian. The lowstand at the base is also documented from the Himalayan Tethys zone by Garzanti et al. (1995). A strong transgressive trend is observed in the Middle Anisian with deposition of a thin pelagic limestone interval followed by siliceous shales and radiolarian cherts. Hallam (1996) also reports an eustatic sea level rise during the Anisian.

The UAA-2.2 cycle starts near the Anisian/Ladinian boundary with a condensed interval made up of siliceous shales and minor siliceous limestone beds without any indication of previous lowstand deposits. The shales grade into a calcareous interval, with filament-bearing calcarenites at the top of the cycle. The calcarenites correspond stratigraphically to the massive progradation of the Ladinian carbonate platforms of the western Tethys (De Zache et al. 1993; Rüffer & Zühlke 1995).

The remaining Triassic sediment series show three transgressive sequences (equated to the UAA-3.1 / -3.2 / -3.3) which start with terrigenous shales and thin-bedded hemipelagic wake- to packstones and end with thickening-upward sequences made up of allochthonous calcarenites and rare *Halobia*-limestone beds. A single LST is represented at the base of the UAA-3.1 which consists of microbreccias, thin bedded turbidites and shaly interbeds. This distinct lowstand is a Tethys-wide phenomenon which corresponds to the Muschelkalk/Keuper boundary of the European epicontinental Triassic (Aigner & Bachmann 1992). It also marks a cessation in the carbonate platform development in the western Tethys (e.g. Bosellini 1996). The onset of the UAA-3.1 cycle is also recorded in an analogue stratigraphic position in the Indian Himalayas by a drastic change from pelagic limestones to siliciclastic deposition (Garzanti et al. 1995). The base of the UAA-3.2 cycle is stratigraphically close to the "Reingrabener Wende" in the Northern Calcareous Alps (Schlager & Schollenberger 1974) which is commonly found along the northern Tethys margin and which is marked by a widespread break in carbonate deposition followed by clastic deposits of the Lunz Formation (Bechstädt & Schweizer 1991). The TST and HST of the UAA-3.2 and UAA-3.3 cycles are widely documented in Late Carnian and Early Norian platform to basin transitions of the western Tethys (Schlaf et al. 1997; Krystyn & Lein 1996).

Carbon and oxygen isotope record of the Southern Tethys during the Triassic

Carbon isotopic variations in marine carbonate rocks can provide important information on stratigraphic relationships and paleoenvironments. Many stable isotope studies have focused on the Permian/Triassic boundary and within the Early Triassic, in contrast to the remainder of the Triassic which has been little studied. Compared with the number of data available on the micro-plates of Cimmeria and the northern edge of Gondwanaland (e.g. the Cimmerides in S–E Asia and Europe), few data exist for the southern Tethyan margin. Carbon isotope profiles from this study were compared to determine the general pattern of carbon isotope variation in the Tethys Sea. Atudorei & Baud (1997) presented a summary of Triassic carbon isotope stratigraphies and discussed their potential use for stratigraphic correlation. Three positive carbon isotope events have been recorded in the Triassic. Atudorei & Baud (1997) correlate the events at the Smithian/Spathian- and the Spathian/Anisian boundaries with pulses of increased carbon burial, as they are coincident with reported radiation events. The Spathian/Anisian-event was interpreted to be global in nature (Atudorei & Baud 1997).

With the exception of the strongly positive values at the base, the isotopic record of the Sal section lies within the range of normal marine carbonates. Noteworthy is the increase of $\delta^{13}C$ values in the Spathian with a maximum in the Late Spathian, followed by the shift from positive to negative values at the Spathian/Anisian boundary. We interpret this $\delta^{13}C$ signal to be original because no relation between $\delta^{13}C$ and the $\delta^{18}O$ values is observed. This large positive excursion could be a chemostratigraphic marker for the Spathian/Anisian boundary. The peak indicates increased organic carbon burial as suggested by Atudorei & Baud (1997), and a major radiation event at the Spathian/Anisian boundary (Hallam 1996). The drastic drop from high positive to negative $\delta^{13}C$ values can be used as an indicator for oceanic productivity and faunal diversity related to changes of sea level (Baud et al. 1989). The negative values indicate a significant decrease in organic carbon burial rates (Burns & Matter 1993). A similar large decrease in $\delta^{13}C$ values occurs at the Permian/Triassic boundary (Baud et al. 1996). This distinct event, which is documented world-wide, was attributed to large scale regression and/or to a major drop in oceanic productivity at the end of the Permian (Holser & Magaritz 1987).

After the large shift to negative $\delta^{13}C$ values at the Spathian/Anisian boundary, the data show a long-term gradual increase in $\delta^{13}C$ beginning in the Anisian and continuing during the Carnian up to the Early Norian. A similar trend was observed by Atudorei & Baud (1997) and Böhm & Gawlick (1997). Superimposed upon this general trend are a number of minor isotopic excursions where coherent $\delta^{18}O$ and $\delta^{13}C$ changes suggest these small events may be diagenetic in origin. Overall, the Anisian through Norian is characterised by a gradual increase in $\delta^{13}C$. Additional data over this time range were published by Steuber (1991) for the Helicon Mountains in Greece. In this section, no significant $\delta^{13}C$ excursions were measured. Steuber's $\delta^{13}C$ values for the Late Triassic confirm our positive carbon isotope values for the Carnian and Early Norian.

Evolution of the Triassic Batain Basin

The occurrence of Triassic deep water deposits, pelagic limestones, radiolarian cherts and calciturbidites in the Batain Basin records the existence of a broad Triassic marine basin along the NE coast of Oman. The sedimentary record of the Batain series starts with reefal and intraplatform basinal rocks of the Permian Qarari Formation (Immenhauser et al. 1998) deposited in a Middle to Late Permian shelf basin. The sedimentological characteristics and the mixed neritic to pelagic fossil assemblages of the following Sal succession indicate an eastward expanding marine basin and continued deepening of the basin due to a widening of the Batain embayment in the Triassic. From our data we suggest that a shallow Batain Basin already existed in the Early Permian, but did not reach greater water depths prior to the Middle Triassic. It remained in a relatively stable position without major tectonic and sedimentary changes until the Early Jurassic.

The here described Triassic sediments in the Batain Plain reflect a relatively proximal position in the basin with associated isochronal and lateral facies changes and sedimentary cycles (Fig. 7). The original palaeogeographic setting of the basin remained intact despite deformation during thrusting of the Sal sediments onto the eastern edge of Arabia. Both, the geographic setting (Fig. 1) and the facies distribution of the sections reveal a basin polarity from distal (ESE) to proximal (WNW) (Fig. 7). Only the primary position of section 4 is uncertain. Though presently located in an intermediate position, this section contains a proximal facies and we, therefore, attribute it to the proximal part of the basin (Fig. 7).

The depositional environments of the Batain embayment during the Triassic may bear resemblance to those of the Sumeini Group (Watts & Garrison 1986) and the Hamrat Duru Group in the Oman Mountains (Cooper 1990; Béchennec et al. 1990). Sediment series similar or identical to those of the Mudstone Member for example have been called platy limestones by Blendinger (1988) or the Upper Al Jil Member by Béchennec et al. (1992a). In the Maqam Formation of the Sumeini Group (Watts & Garrison 1986), the C- and D-members resemble the Mudstone Member and the E-member of our Chert Member. Nevertheless, based on the differing later lithostratigraphic history we assume a different geodynamic evolution and basin architecture for the Batain Basin. During the Early Triassic the basin was dominated by an homoclinal carbonate ramp with a change to a distally steepened ramp in the Anisian time. During the time span from the Ladinian to Norian the increase of siliceous shales, pelagic limestones and proximal calciturbidites with erosion and reworking of the substratum indicate a slope and bypass margin. In the Rhaetian, sedimentation of calcareous sandstones and terrigenous shales predominated in the eastern Batain basin. This may indicate the Rhaetian regression (Hallam & Wignall 1997) which is also documented from the Hawasina Basin (Murris 1980; Bernoulli & Weissert 1987; Bernoulli 1988; Bernoulli et al. 1990).

5. Summary and Conclusions

1. The results from the Triassic sections studied within the Batain Nappes confirm that their thrusting direction differed from that of the Hawasina series (Immenhauser et al. 1998, Schreurs et al. 1999) and that the Batain Basin existed between Arabia and India from the Early Permian onwards.
2. The lithostratigraphy and the new biostratigraphic data allow definition of a type-section (Fig. 4A–E) for the proximal Triassic Batain embayment, represented by the Sal Formation.
3. The sequence stratigraphy of the East Arabian Batain Triassic (Fig. 8) shows well developed sedimentation cycles from the East Arabian (southern Tethys) margin, which are identical to those of the Indian margin for the Early to Middle Triassic (Garzanti et al. 1995). This could be an indication that the sedimentation and the sea level changes at the Southern Tethys margin were controlled by supra regional systems.
4. The $\delta^{13}C$ isotope curve from the type-section (Fig. 8) shows a large positive peak in the Late Scythian which was also found by Adutorei & Baud (1997) in a composite section from the northern Tethys margin in Rumania. This $\delta^{13}C$ peak corresponds with a general sea level drop in the southern Tethys at the end of transgressive 2nd order cycle (UAA-1). We believe that the Spathian-Anisian event can be used as a global stratigraphical marker, but it needs further confirmation from other Neotethyan sections.
5. The basin architecture and the absence of a clear indication of Permo-Triassic sea mounts and/or oceanisation with a rift phase between Arabia and India point to a different geodynamic evolution of the Batain Basin as compared to that of the Hawasina Basin. The type-section of the Sal Formation is, therefore, seen as a general reference for the Triassic evolution of the Batain segment along the southern Tethys margin.

Acknowledgements

The present paper is a result of a geological mapping and research program (sheets Sur and Al Ashkahrah 1:100'000) of the Universities of Berne and Geneva supported by the Swiss National Foundation (projects No. 20-43'056.95 T.P. and No. 20-50577.97 L. Z.), and the Director General of Minerals, Mohammed Bin Hussein Bin Kassim, Ministry of Commerce and Industry, Sultanate of Oman, and Dr. Hilal Al Azry, Director of the Geological Survey. We are grateful to H. Kozur for determining the Permian conodonts and appreciate the constructive remarks of E. Gnos, A. Immenhauser, G. Roselle, N. Scherrer and Lina Bobade.

REFERENCES

AIGNER, T. & BACHMANN, G. H. 1992: Sequence-stratigraphic framework of the German Triassic. Sediment. Geol. 80, 115–135.

ALLEMANN, F. & PETERS, T. 1972: The Ophiolite-Radiolarite Belt of the North-Oman Mountains. Eclogae geol. Helv. 65, 657–697.

ATUDOREI, V. & BAUD, A. 1997: Carbon isotope events during the Triassic. Albertiana 20, 45–49.

BAUD, A., MAGARITZ, M. & HOLSER, W. T. 1989: Permian-Triassic of the Tethys: Carbon isotope studies. Geol. Rdsch. 78/2, 649–677.

BAUD, A., ATUDOREI, V., & SHARP, Z. 1996: Late Permian and Early Triassic evolution of the Northern Indian margin: carbon isotope and sequence stratigraphy. Geodyn. Acta (Paris) 9, 2, 57–77.

BEAUCHAMP, W. H., RIES, A. C., COWARD, M. P. & MILES, J. A. 1995: Masirah Graben, Oman: A hidden Cretaceous Rift System? Bull. amer. Assoc. Petroleum Geol. 79, 864–879.

BÉCHENNEC, F. 1987: Géologie des nappes Hawasina dans les parties orientale et centrale des Montagnes d'Oman. Thèse Doct. d'État, Université P. et M. Curie, Paris VI, Bur. Rech. Géol. Min., Document n° 127, Orléans, France, 417p.

BÉCHENNEC, F., LE MÉTOUR, J., RABU, D., BOURDILLON-DE-GRISSAC, C., DE WEVER, P. & VILLEY, M. 1990: The Hawasina Nappes: stratigraphy, palaeogeography and structural evolution of a fragment of the south-Tethyan passive continental margin. In: The Geology and Tectonics of the Oman Region. (Ed. by ROBERTSON, A. H. F., SEARLE, M. P. & RIES, A. C.). Spec. Publ. geol. Soc. London 49, 213–224.

BÉCHENNEC, F., ROGER, J., LE MÉTOUR, J. & WYNS, R. 1992a: Geological Map of Seeb, sheet NF 40–03, scale 1:250'000 with explanatory notes. Directorate General of Minerals, Oman Ministry of Petroleum and Minerals, Muscat.

BÉCHENNEC, F., ROGER, J., CHEVREL, S. & LE MÉTOUR, J. 1992b: Geological Map of Al Ashkharah, sheet NF 40–12, scale 1:250'000 with explanatory notes. Directorate General of Minerals, Oman Ministry of Petroleum and Minerals, Muscat.

BECHSTÄDT, T. & SCHEIZER, T. 1991: The carbonate-clastic cycles of the East-Alpine Raibl Group: Results of third order sea-level fluctuations in the Carnian. Sediment. Geol. 70, 241–270.

BERNOULLI, D. & WEISSERT, H. 1987: The upper Hawasina nappes in the central Oman Mountains: stratigraphy, palinspastics and sequence of the nappe emplacement. Geodyn. Acta 1, 47–58.

BERNOULLI, D., WEISSERT, H. & BLOME, C. D. 1990: Evolution of the Triassic Hawasina Basin, Central Oman Mountains. In: The Geology and Tectonics of the Oman Region. (Ed. by ROBERTSON, A. H. F., SEARLE, M. P. & RIES, A. C.). Spec. Publ. geol. Soc. London 49, 189–202.

BLENDINGER, W. 1988: Permian to Jurassic Deep Water Sediments of the Eastern Oman Mountains: Their Significance for the Evolution of the Arabian Margin of the South Tethys. Facies 19, 1–32.

BLOME, C. 1984: Upper Triassic Radiolaria and radiolarian zonation from western North America. Bull. amer. Paleont. 1–88, Pl. 1–17.

BOSELLINI, A. 1996: Geologia delle Dolomiti. Athesia Bozen, 1–192.

BÖHM, F. & GAWLICK, H.-J. 1997: Late Triassic carbon isotope excursion in pelagic limestones of the Northern Calcareous Alps. In: Abstr. 18th Reg. Eur. Meet. Sediment. Gaea heidelbergensis 3, 79–80.

BURNS, S. J. & MATTER, A. 1993: Carbon isotopic record of the latest Proterozoic from Oman. Eclogae geol. Helv. 86/2, 595–607.

COOPER, D. J. W. 1987: Hamrat Duru Group: revised stratigraphy of a Mesozoic deep-water passive margin in the Oman Mountains. Geol. Mag. 124, 157–164.

COOPER, D. J. W. 1990: Sedimentary evolution and paleogeographical reconstruction of the Mesozoic continental rise in Oman: evidence from the Hamrat Duru Group. In: The Geology and Tectonics of the Oman Region. (Ed. by ROBERTSON, A. H. F., SEARLE, M. P. & RIES, A. C.). Spec. Publ. geol. Soc. London 49, 161–187.

DE ZANCHE, V., GIANOLLA, P., MIETTO, P., SIORPAES, C. & VAIL, P. R. 1993: Triassic Sequence Stratigraphy in the Dolomites (Italy). Mém. Sci. géol. (Strasbourg) 45, 1–27.

DUMITRICA, P. 1982: Triassic Oertlispongidae (Radiolaria) from Eastern Carpathians and Southern Alps. Dari de Seama ale sedintelor, Inst. Geol. and Geofiz. Bucuresti 67(3), 57–74, pls. 1–12.

GALLET, Y., KRYSTYN, L. & BESSE, J. 1998: Upper Anisian to Lower Carnian magnetostratigraphy from the Northern Calcareous Alps (Austria). J. geophys. Res. 103 B1, 605–621.

GALLET, Y., BESSE, J., KRYSTYN, L., THEVENIAUT, H. & MARCOUX, J. 1994: Magnetostratigraphy of the Mayerling section (Austria) and Erenkolu (Turkey) section: Improvement of the Carnian (Late Triassic) magnetic polarity time scale. Earth and planet. Sci. Lett. 125, 173–191.

GIANOLA, P. & JACQUIN, T. 1998: Triassic sequence stratigraphic framework of Western European basins. SEPM Spec. Publ. 50, 643–650.

GRADSTEIN, M., AGTERBERG, F. P., OGG, J. G., HARDENBOL, J., VAN VEEN, P., THIERRY, J. & HUANG, Z. 1994: A Mesozoic time scale. J. geophys. Res. 99 (B12), 24,051–24,074.

GARZANTI, E., JADOUL, F., NICORA, A. & BERRA, F. 1995: Triassic of Spiti (Tethys Himalaya, N India). Riv. ital. Paleont. (Stratigr.) 101 (3), 267–300.

GLENNIE, W. K., BOEUF, M. G. A., HUGHES-CLARKE, M. W., MOODY-STUART, M., PILAAR, W. & REINHARDT, B. M. 1974: Geology of the Oman Mountains. Verh. geol.-mijnbouwkd. Genoot. Nederl., Transactions 31, The Hague, Shell Research BV.

HALLAM, A. 1996: Major Bio-Events in the Triassic and Jurassic. In: Global Events and Event Stratigraphy in the Phanerozoic. (Ed. by WALLISER, O. H.). Springer Verlag, 265–283.

HALLAM, A. & WIGNALL, P. B. 1997: Mass extinctions and their aftermath. Oxford University Press.

HAQ, U. B. 1991: Sequence stratigraphy, sea level change, and significance for the deep sea. In: Sedimentation, tectonics and eustasy; sea-level changes at active margins. (Ed. by MACDONALD, D. I. M.). Spec. Publ. Int. Ass. Sedim. Blackwell Oxford 12, 3–39.

HAQ, B. U., HARDENBOL, J. & VAIL, P. R. 1987: Chronology of fluctuating sea levels since the Triassic (250 million years ago to present). Science 235, 1156–1166.

HAQ, B. U., HARDENBOL, J. & VAIL, P. R. 1988: Mesozoic and Cenozoic chronostratigraphy and cycles of sea-level change. In: Sea-level changes an integrated approach. (Ed. by WILGUS, C. K., HASTING, B. S., ROSS, C. A., POSAMENTIER, H. W., VAN-WAGONER, J. & KENDALL, CH. G.). SEPM Spec. Publ. 42, 71–108.

HOLSER, W. T. & MAGARITZ, M. 1987: Events near the Permian-Triassic boundary. Mod. Geol. 11, 155–180.

IMMENHAUSER, A., SCHREURS, G., PETERS, T., MATTER, A., HAUSER, M. & DUMITRICA, P. 1998: Stratigraphy, sedimentology and depositional environment of the Batain Group. Eclogae geol. Helv. 91, 217–235.

KOZUR, H. 1996: The systematic position of *Pseudoertlispongus* Lahm (Radiolaria) and description of some new Middle Triassic and Liassic radiolarian taxa. Geol. Paläont. Mitt. Innsbruck Sonderbd. 4, 287–299.

KOZUR, H. & MOSTLER, H. 1994: Anisian to Middle Carnian radiolarian zonation and description of some stratigraphically important radiolarians. Geol. Paläont. Mitt. Innsbruck Sonderbd. 3, 39–255.

KOZUR, H. & MOSTLER, H. 1996: Longobardian (Late Ladinian) Oertlispongidae (Radiolaria) from the Republic of Bosnia-Hercegovina and the stratigraphic value of advanced Oertlispongidae. Geol. Paläont. Mitt. Innsbruck Sonderbd. 4, 105–193.

KRYSTYN, L. 1980: Triassic conodont localities of the Salzkammergut region (Northern Calcareous Alps). Abh. Geol. Bundesanst. Wien 35, 61–98.

KRYSTYN, L. & LEIN, R. 1996: Triassische Becken- und Platformsedimente der östlichen Kalkalpen. Abh. Geol. Bundesanst. Wien 33, 23.

LAHM, B. 1984: Spumellarienfaunen (Radiolaria) aus den mitteltriassischen Buchensteiner-Schichten von Recoaro (Norditalien) und den obertriassischen Reiflingerkalken von Grossreifling (Österreich): Systematik, Stratigraphie. Münchner Geowiss. Abh. 1A, 160, pl. 19.

MARQUER, D., PETERS, T. & GNOS, E. 1995: A new structural interpretation for the emplacement of the Masirah Ophiolite (Oman): A main Paleocene intra-oceanic thrust. Geodyn. Acta 8, 13–19.

MCCREA, J. M. 1950: Isotopic chemistery of carbonates and a paleotemperature scale. J. Chem. Phys. 18, 849–857.

NICORA, A. 1977: Lower Anisian platform conodonts from the Tethys and Nevada. Taxonomic and stratigraphic revision. Palaeontographica 157, 88–107.

MURRIS, R. J. 1980: Middle East: Stratigraphic evolution and oil habitat. Bull. amer. Assoc. Petroleum Geol. 64, 597–618.

ORCHARD, M. 1995: Taxonomy and correlation of Lower Triassic (Spathian) segminate conodonts from Oman and revision of some species of Neospathodus. J. Paleont. 69/1, 110–122, Tulsa.

READ, J. F. 1982: Carbonate platforms of passive (extensional) continental margins: Types, characteristics and evolution. Tectonophysics 81, 195–212.

ROBERTSON, A. H. F. & SEARLE, M. P. 1990: The northern Oman Tethyan continental margin: stratigraphy, structure, concepts and controversis. In: The Geology and Tectonics of the Oman Region. (Ed. by ROBERTSON, A. H. F., SEARLE, M. P. & RIES, A. C.). Spec. Publ. geol. Soc. London 49, 3–25.

ROGER, J., BÉCHENNEC, F., JANJOU, D., LE MÉTOUR, J., WYNS, R. & BEURRIER, M. 1991: Geological Map of Ja'alan sheet NF 40–8E, scale 1:100'000 with explanatory notes. Directorate General, Oman Ministry of Petroleum and Minerals, Muscat.

RÜFFER, T. & ZÜHLKE, R. 1995: Sequence stratigraphy and sea-level changes in the Early to Middle Triassic of the Alps: a global comparison. In: Sequence Stratigraphy and Depositional Response to Eustatic, Tectonic and Climatic Forcing. Kluver Amsterdam, 161–207.

SCHLAF, J., LEIN, R. & KRYSTYN, L. 1997: Sequence stratigraphy of Upper Triassic carbonate platform margins in the Julian Alps (Slovenia). Gaea heidelbergensis 3, 303–304.

SCHLAGER, W. 1997: On the definition of "Ramp". Gaea heidelbergensis 3, 304.

SCHLAGER, W. & SCHOLLENBERGER, W. 1974: Das Prinzip stratigraphischer Wenden in der Schichtfolge der Nördlichen Kalkalpen. Mitt. geol. Ges. Wien 67, 165–193.

SCHLAGER, W., REIJMER, J. J. G. & DROXLER, A. 1994: Highstand shedding of carbonate platforms. J. sediment. Res. 64/B, 270–281.

SCHLAGER, W. & CAMBER, O. 1986: Submarine slope angles, drowning unconformities, and shelf-erosion of limestone escarpments. Mem. geol. Soc. Amer. 14/9, 762–765.

SCHREURS, G. & IMMENHAUSER, A. 1999: WNW-Directed Obduction of the Batain Group on the East Oman Continental Margin at the Cretaceous-Tertiary Boundary. Tectonics 18/1, 148–160.

SHACKLETON, R. M., RIES, A. C., BIRD, A. C., FILBRANDT, J. B., LEE, C. W. & CUNNINGHAM, G. C. 1990: The Batain Melange of NE Oman. In: The Geology and Tectonics of the Oman Region. (Ed. by ROBERTSON, A. H. F., SEARLE, M. P. & RIES, A. C.). Spec. Publ. geol. Soc. London 49, 673–696.

STEUBER, T. 1991: Conodont stratigraphy, depositional environments and stable isotope composition of the Triassic in the Helicon Mountains (Beotia, Greece). Bul. geol. Soc. Greece 25/2, 415–528.

UROSEVIC, D. 1988: Microfossils from the Triassic of the Inner Belt of the Yugoslavian Carpatho-Balkanides. Annales géologiques de la Péninsule Balkanique 52, 371–379.

VAIL, P. R., AUDEMARD, F., BOWMAN, S. A., EISNER, P. N. & PEREZ-GRUZ, C. 1991: The Stratigraphic Signatures of Tectonics, Eustasy and Sedimentology – an Overview. In: Cycles and Events in Stratigraphy (Chapter 6). (Ed. by EINSELE, G., RICKEN, W. & SEILACHER, A.). Springer-Verlag Berlin, 617–659.

WATTS, K. F. & GARRISON, R. E. 1986: Sumeni Group, Oman-Evolution of a Mesozoic carbonate slope on a South Tethyan continental margin. Sediment. Geol. 48, 107–168.

WYNS, R., BÉCHENNEC, F., LE MÉTOUR, J., ROGER, J. & CHERVEL, S. 1992: Geological map of Sur, sheet NF-40–08, scale 1:250'000 with explanatory notes. Directorate General of Minerals, Oman Ministry of Petroleum and Minerals, Muscat.

ZANINETTI, L., CIARAPICA, G., MARTINI, R. & RETTORI, R. 1990: Paléoécologie des Turriglomines (Foraminifères) dans le Trias de l'Apennin méridional (Basin de Lagonero) Italie. Arch. Sci. Genève 43/2, 295–305.

Manuscript received October 19, 1999
Revision accepted February 6, 2001

Plate 1

Conodonts from the Sal Formation (scale bar represents 100 microns)

Fig. 1. *Norigondolella navicula* (Huckriede). Sample H830
Fig. 2. *Budurovignathus mungoensis* (Diebel). Sample 98/18
Fig. 3a, b. *Gondolella cf. slovenica* Ramovs. Sample H831
Fig. 4. *Neospathodus* cf. *dieneri* (Sweet). Samplel H830
Fig. 5. *Neospathodus* cf. *homeri* (Bender). Sample H836
Fig. 6a, b. *Metapolygnathus carpathicus* (Kozur & Mock). Sample H843
Fig. 7a, b. *Metapolygnathus* communisti Hayashi. Sample H830
Fig. 8a, b. *Neospathodus* cf. *abruptus* Orchard. Sample 98/23
Fig. 9a, b. *Paragondolella inclinata* (Budurov & Stefanov). Sample H836
Fig. 10a, b. *Metapolygnathus nodosus* Hayashi. Sample H833
Fig. 11a, b. *Metapolygnathus carnicus* (Krystyn). Sample H836
Fig. 12a, b. *Metapolygnathus auriformis* (Kovacs). Sample H842
Fig. 13a, b. *Metapolygnathus polygnathiformis* (Budurov & Stefanov). Sample H833
Fig. 14. *Budurovignathus mungoensis (Diebel)*. Sample H835
Fig. 15. *Paragondolella trammeri* (Kozur). Sample 98/17

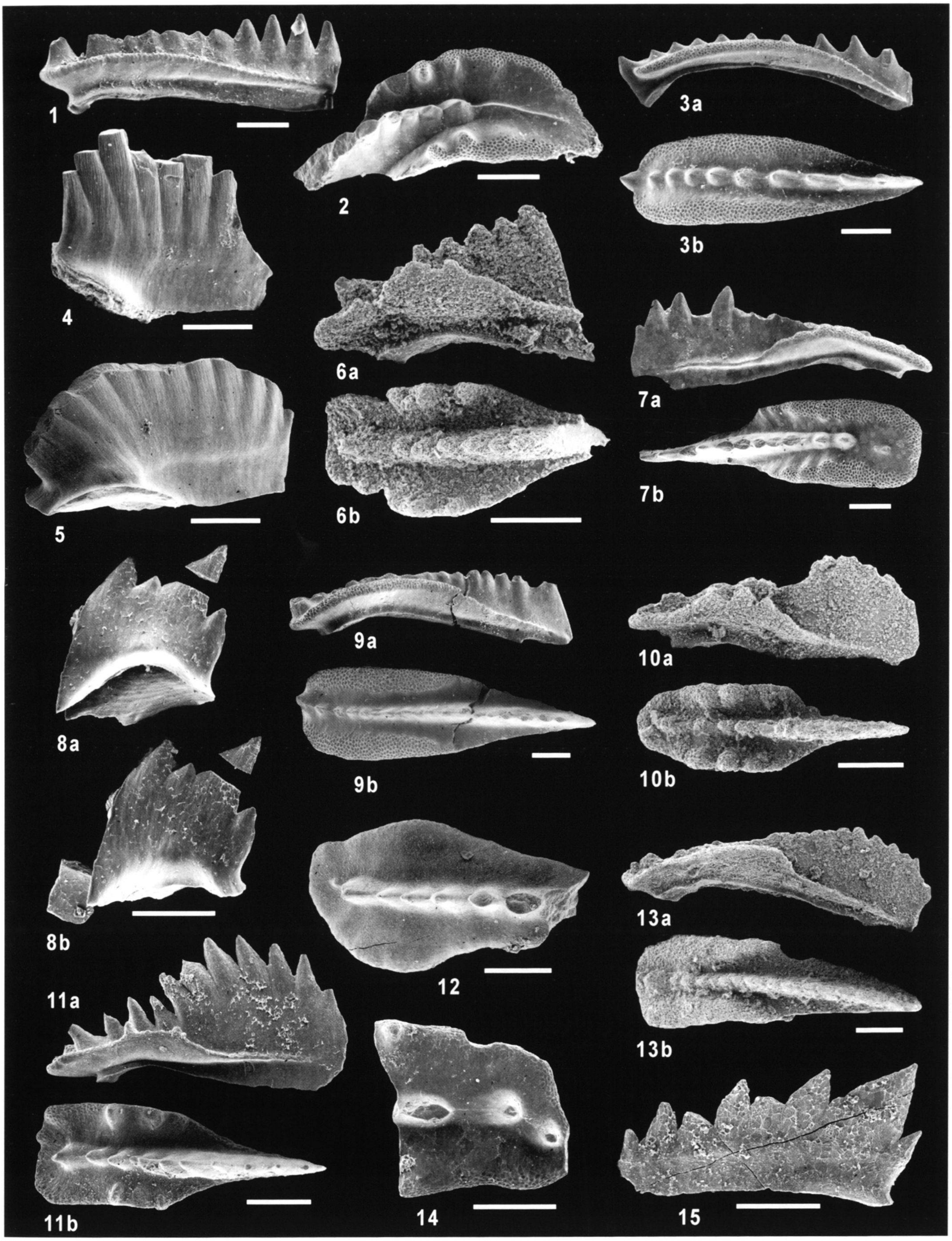
1
2
3a
3b
4
5
6a
6b
7a
7b
8a
8b
9a
9b
10a
10b
11a
11b
12
13a
13b
14
15

Plate 2

A. Radiolarian assemblage of sample H827, upper Illyrian:
1. *Pararchaeospongoprunum cf. hermi* Lahm, x100.
2. *Paroertlispongus multispinosus* Kozur & Mostler, x100.

B. Radiolarian assemblage of sample H828, uppermost Illyrian-lowermost Fassanian:
3. *Paroertlispongus multispinosus* Kozur & Mostler, x120.
4–7. *Paroertlispongus mostleri* Kozur: 4. x120; 5. x120; 6. x120; 7. x140.
8. *Spongopallium hadra* (Sugiyama), x135.
9. *Pseudostylosphaera japonica* (Nakaseko & Nishimura), x90.
10. *Tetra spinocyrtis* (?) n. sp., x270.
11. *Bulbocyrtium* (?) sp., x200.
12. *Plafkerium confluens* Dumitrica, Kozur & Mostler, x150.
13. *Hozmadia* sp., x250.
14. *Paronaella* sp., x100.

C. Radiolarian assemblage of sample P373, lower-middle Fassanian:
15.–16. *Oertlispongus multispinosus* Dumitrica, Kozur & Mostler: 15. x100; 16. x100.
17. *Falcispongus falciformis* Dumitrica, x135.
18.–19. *Oertlispongus inaequispinosus* Dumitrica, Kozur & Mostler: 18. x150; 19. x120.
20. *Baumgartneria stellata* Dumitrica, x135.
21.–22. *Falcispongus calcaneum* Dumitrica: 21. x180; 22. x180.
23. *Falcispongus* sp., x165.
24. *Baumgartneria* sp., x150.
25.–26. *Baumgartneria transita* Kozur & Mostler: 25. x135; 26. x140.
27. *Tiborella magnidentata* Dumitrica, Kozur & Mostler, x150.
28. *Spongopallium hadra* (Sugiyama), x185.
29. *Pararchaeospongoprunum* sp., x150.
30. *Cryptostephanidium* sp., x200.
31. *Eptingium manfredi* Dumitrica, x100.
32. *Cryptostephanidium cornigerum* Dumitrica, x150.
33. *Tiborella* cf. *magnidentata* Dumitrica, Kozur & Mostler, x150.
34. *Hozmadia spinosa* Kozur & Mostler, x250.
35. *Hexacontium* (?) sp., x150.
36.–37. *Pseudostylosphaera japonica* (Nakaseko & Nishimura): 36. x140; 37. x120.
38. *Hozmadia* (?) sp., x150.
39. *Goestlingela ilyrica* Kozur, x200.
40. *Triassocampe scalaris* Dumitrica, Kozur & Mostler, x150.
41. *Pararuesticyrtium fusiformis* (Bragin), x150.

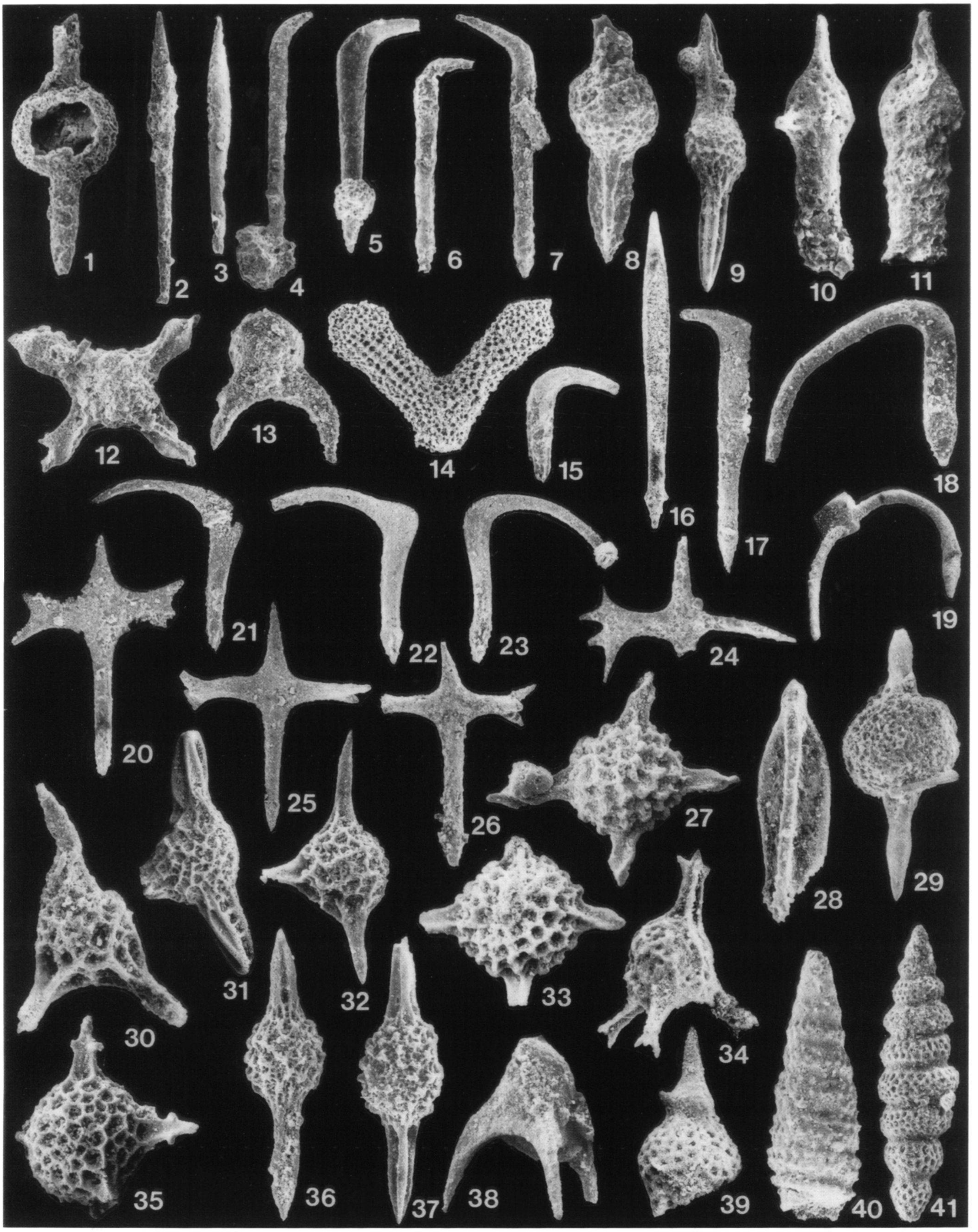

1
2
3
4
5
6
7
8
9
10
11
12
13
14
15
16
17
18
19
20
21
22
23
24
25
26
27
28
29
30
31
32
33
34
35
36
37
38
39
40
41

Plate 3

C. Radiolarian assemblage of sample P373, lower-middle Fassanian:
1. *Planispinocyrtis baloghi* Kozur & Mostler, x230.
2. *Annulotriassocampe campanilis* Kozur & Mostler, x200.
3. *Triassocampe nodosoannulata* (Kozur & Mostler), x170.

D. Radiolarian assemblage of sample A181, Fassanian:
4. *Falcispongus falciformis* Dumitrica, x120.
5.–7. *Turospongus* (?) sp.: 5. x135; 6. x135; 7. x135.
8. *Oertlispongus* cf. *inaequispinosus* Dumitrica, Kozur & Mostler, x135.

E. Radiolarian assemblage of sample A119, lower Longobardian:
9. Oertlispongid, gen. et sp. indet., x135.
10. *Archaeocenosphaera* sp., x140.
11. *Parasepsagon* (?) sp., x135.
12. Spumellarian (?), gen. et sp. indet., x200.
13. *Sepsagon* (?) *robustus* Lahm, 14056, x135.
14. Nassellarian, gen. et sp. indet., x150.
15. *Pararuesticyrtium* (?) sp., inner cast, x200.
16. *Pseudostylosphaera canaliculata* (Bragin), x100.
17. *Pseudostylosphaera* sp. B of Yeh 1992, x100.
18. Spumellarian (?), gen. et sp. indet., x200.
19. *Striatotriassocampe* cf. *laeviannulata* Kozur & Mostler, x150.

F. Radiolarian assemblage of sample P378, upper Longobardian/lower Cordevolian:
20. *Triassistephanidium anisicum* Kozur, Krainer & Mostler, x200.
21. *Dumitricasphaera* sp., x150.
22. *Vinassaspongus subsphaericus* Kozur & Mostler, x165.
23. Spumellarian, gen. et sp. indet., x200.
24. *Archaeosemantis pterostephanus* Dumitrica, x100.
25. *Bogdanella* cf. *trentana* Kolar-Jurkovsek, x200.
26. *Ornatisaturnalis translatus* Mostler & Krainer, x130.
27, 32. *Muelleritortis koeveskalensis* Kozur: 27. x100; 32. x100.
28. *Tritortis kretaensis* (Kozur & Krahl), x120.
29, 31, 33. *Tritortis* cf. *kretaensis* (Kozur & Krahl): 29. x100; 31. x100; 33. x100.
30. *Spongoserrula rarauana* Dumitrica, x100.
34. *Tritortis dispiralis* (Bragin), x150.
35. Nassellarian, gen. et sp. indet., x200.
36. *Hsuum* (?) aff. *cordevolicum* Kozur & Mostler, x250.
37. *Xiphotheca* (?) *dimidiata* Bragin, x150.
38. *Triassocampe* (?) sp., x150.

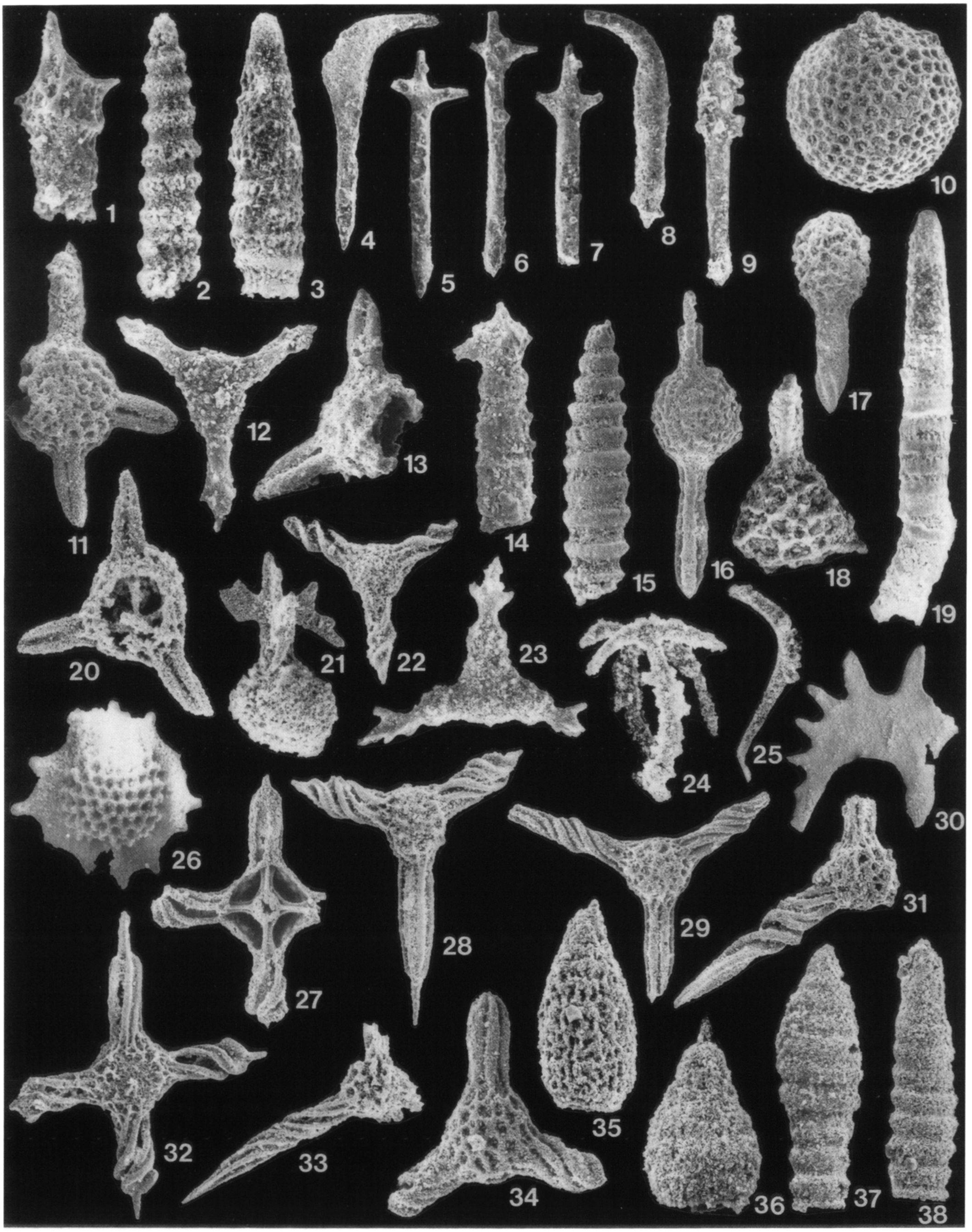
1
2
3
4
5
6
7
8
9
10
11
12
13
14
15
16
17
18
19
20
21
22
23
24
25
26
27
28
29
30
31
32
33
34
35
36
37
38

Plate 4

F. Radiolarian assemblage of sample P378, upper Longobardian/lower Cordevolian: 1.-2. *Corum* (?) sp.: 1. x200; 2. x150.

G. Radiolarian assemblage of sample H844, Middle-Upper Carnian:

3. *Spongostylus carnicus* Kozur & Mostler, x120.
4. *Pseudostylosphaera* (?) sp., x150.
5. *Zhamoidasphaera* cf. *proceruspinosa* Lahm, x165.
6. Spumellarian, gen. et sp. indet., x135.

7.–8. *Capnuchosphaera deweveri* Kozur & Mostler: 7. x200; 8. x120.

9. *Kahlerosphaera* sp., x135.
10. *Paronaella* (?) sp., x85.
11. *Archaeocenosphaera* sp., x165.

12.–13. *Capnuchosphaera* cf. *silviensis* Blome: 12. x120; 13. x120.

14. *Kahlerosphaera philippinensis* Yeh, x120.
15. *Capnuchosphaera* cf. *tortuosa* Yeh, x120.

16.–17. *Capnodoce* (?) cf. *venusta* Pessagno: 16. x180; 17. x165.

18. *Capnuchosphaera* sp., x120.

19., 25. *Capnuchosphaera colemani* Blome: 19. x120; 25. x135.

20.–24. *Capnuchosphaera* spp.: 20. x120; 21. x120; 22. x135; 23. x120;24. x120.

26.–27. *Capnuchosphaera* cf. *lea* De Wever: 26. x120; 27. x135.

28.–29. *Poulpus pansus* De Wever: 28. x200; 29. x200.

30. *Triassocampe sulovensis* Kozur & Mock, x200.
31. *Xiphotheca karpenissionensis* De Wever, x165.
32. *Trialatus* cf. *megacornutus* Yeh, x200.
33. *Latium mundum* Blome, x200.

34.–35. *Capnuchosphaera* spp.: 34. x120; 35. x135.

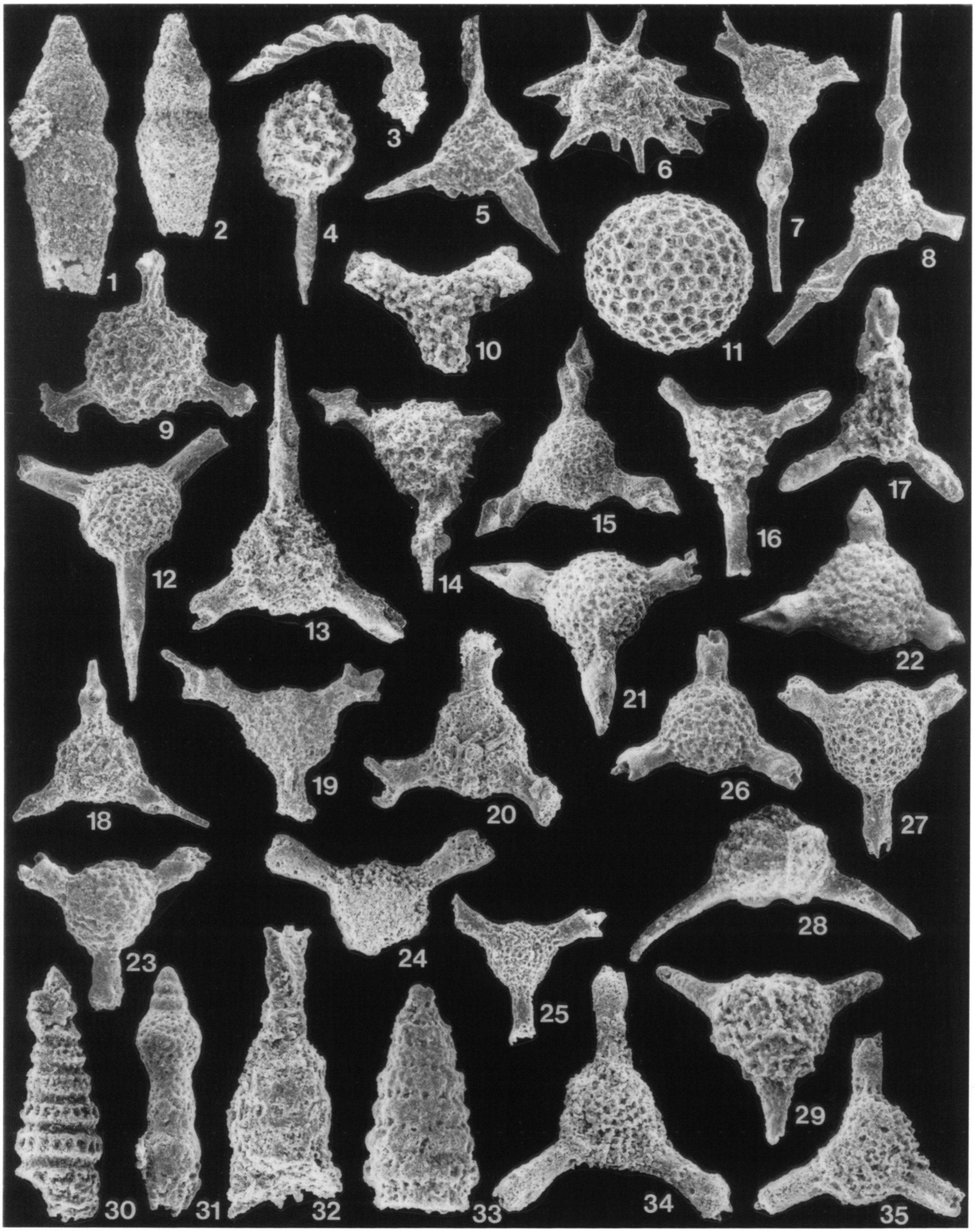
1
2
3
4
5
6
7
8
9
10
11
12
13
14
15
16
17
18
19
20
21
22
23
24
25
26
27
28
29
30
31
32
33
34
35

Plate 5

H. Radiolarian assemblage of sample A198, upper Carnian-lower Norian:
1. *Sarla* cf. *vizcainoensis* Pessagno, x135.
2. *Sarla* (?) sp., x150.
3. *Capnuchosphaera* cf. *theloides* De Wever, x165.
4. *Capnuchosphaera colemani* Blome, x120.
5. *Capnuchosphaera* cf. *soldierensis* Blome, x135.
6.–7. *Capnuchosphaera crassa* Yeh: 6. x135; 7. x135.
8. *Pachus* (?) sp., x250.
9. *Canoptum* sp. A of Blome 1984, x180.
10. Nassellarian, gen. et sp. indet., x250.
11. *Canesium* (?) sp., x200.
12. *Trialatus* sp., x135.

I. Radiolarian assemblage of sample A125, lower Norian:
13., 16. *Capnodoce* cf. *anapetes* De Wever: 13. x150; 16. x150.
14. *Capnodoce* cf. *antiqua* Blome, x150.
15. *Capnodoce* (?) sp., x120.
17.–18. *Capnuchosphaera* cf. *theloides* De Wever: 17. x120; 18. x120.
19. *Capnuchosphaera* cf. *silviesensis* Blome, x120.
20. *Xiphotheca* (?) sp., inner cast, x150.
21., 27. *Canoptum* (?) sp., inner casts: 21. x200; 27. x180.
22.–23. *Triassocampe* sp., inner cast: 22. x200, 23. same, detail of cephalic structure, x600.
24., 26. *Canesium* (?) cf. *cucurbita* Sugiyama: 24. detail of Fig. 26 showing the cephalic structure, x1000; 26. x200.
25. *Latium mundum* Blome, x135.
28.–29. *Xiphotheca rugosa* Bragin: 28. x150; 29. x150.

J. Radiolarian assemblage of sample H621, lower-middle Norian:
30. *Syringocapsa* sp., x120.
31. *Latium paucum* Blome, x135.
32. *Castrum perornatum* Blome, x165.
33.–34. *Castrum* (?) sp.: 33. x140; 34. x140.
35. *Latium mundum* Blome, x180.

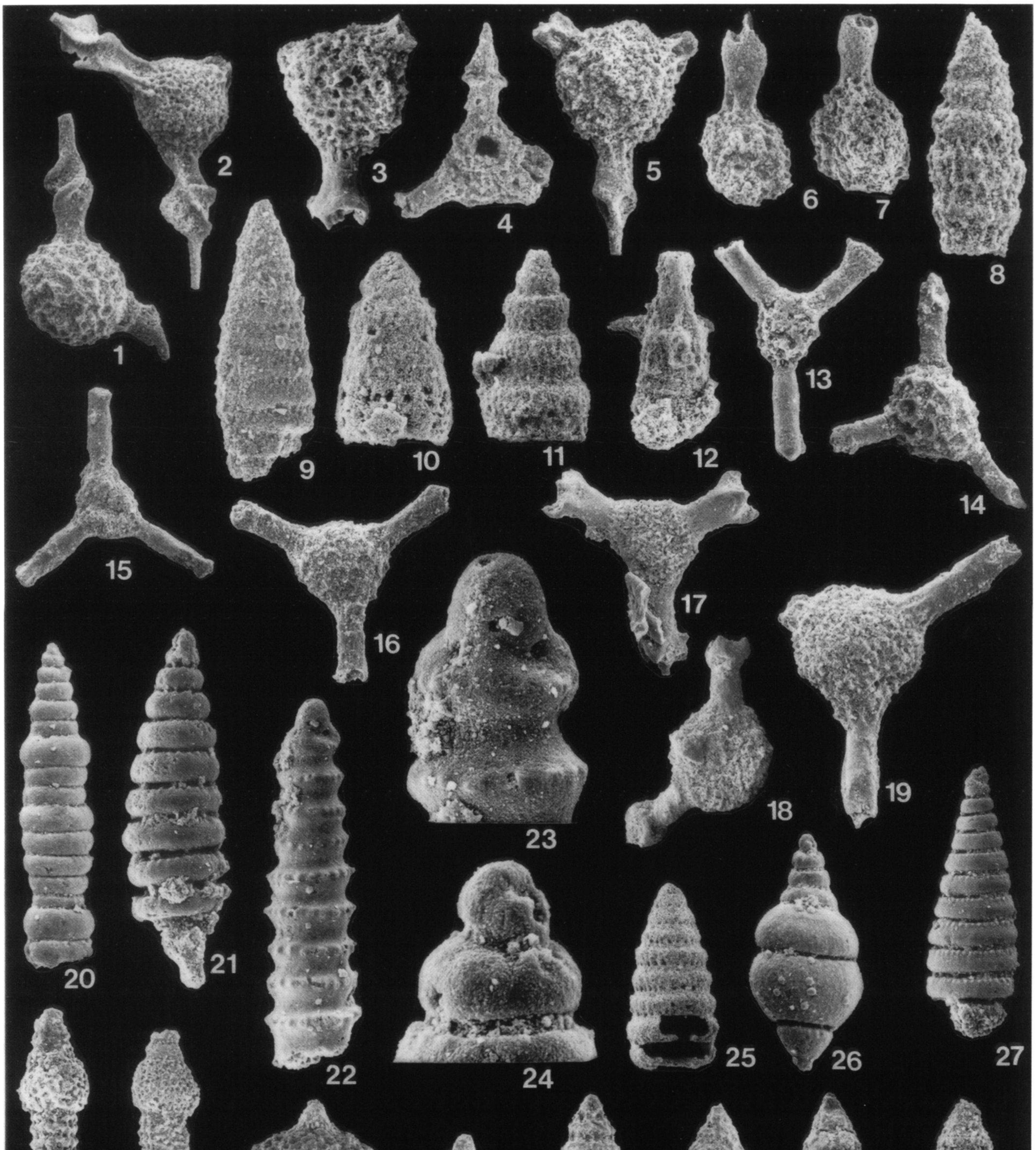
1
2
3
4
5
6
7
8
9
10
11
12
13
14
15
16
17
18
19
20
21
22
23
24
25
26
27
28
29
30
31
32
33
34
35

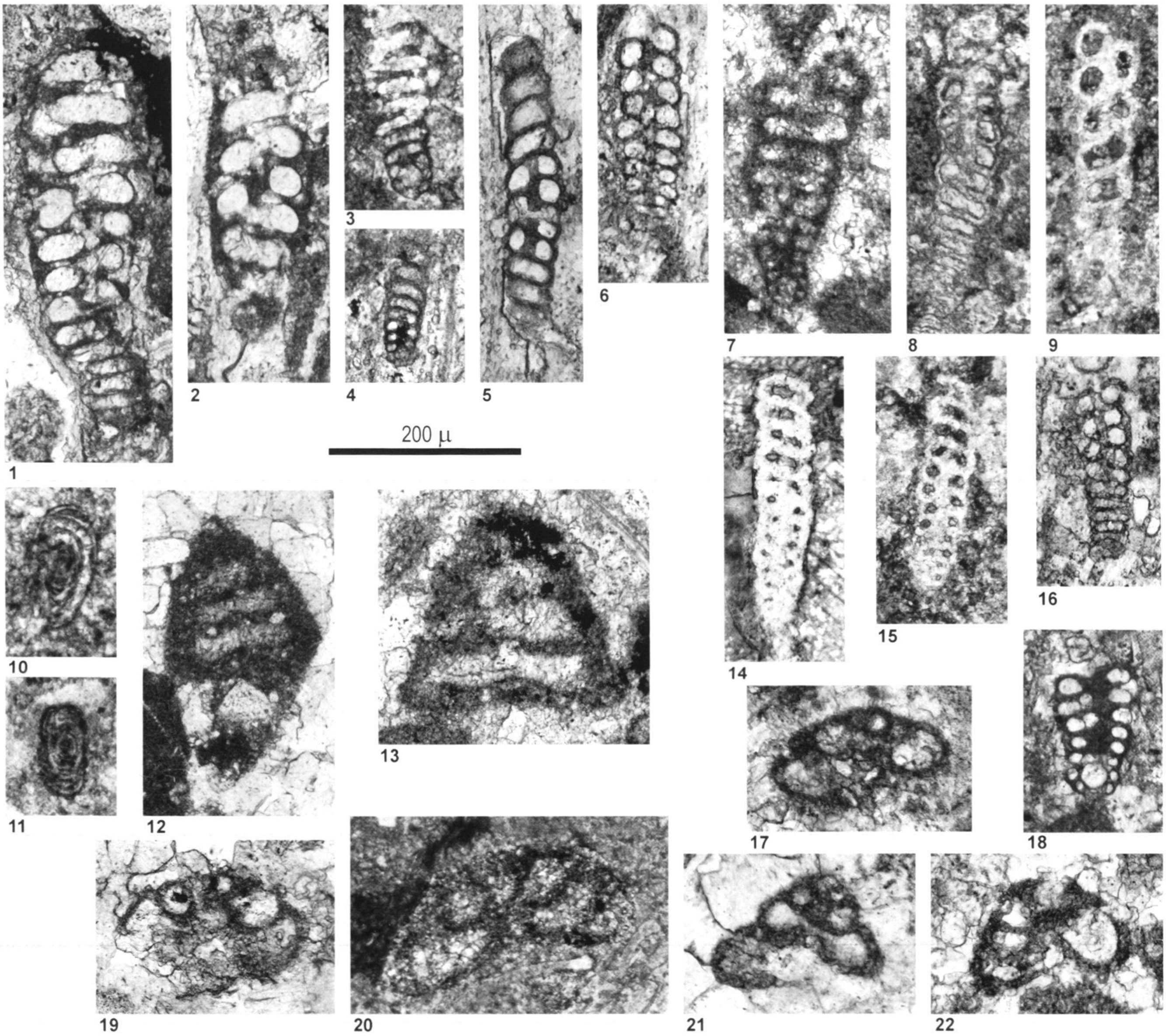

Plate 6

Fig. 1., 2. *Turriglomina* aff., *T scandonei* Zaninetti et al. Sample Mb95.
Fig. 3.–7. *Turriglomina* aff., *T magna* (Urosevic). Samples: Mb95 (3); Mb182 (4-6); H511 (7).
Fig. 8.–9., 14.–16. *Turriglomina mesotriasica* (Koehn-Zaninetti). Samples: H566 (8), overgrowth specimen; H614 (9,15), overgrowth specimens; H5/7,(14) silicified specimen; Mb 182 (16).
Fig. 10.–11. *Gsollbergella spiroloculiformis* (Oraveczne-Scheffer). Sample H614
Fig. 12.–13. *Palaeolituonella meridionalis* (Luperto). Samples: Mb100 (12); H5/10 (13).
Fig. 17., 19.–22. *Duotaxis* sp. Samples: H5/1 (17, 21-22); Mb127 (19); Mb 151 (20).
Fig. 18. *Turriglomina conica* (He Yan). Sample Mb95.

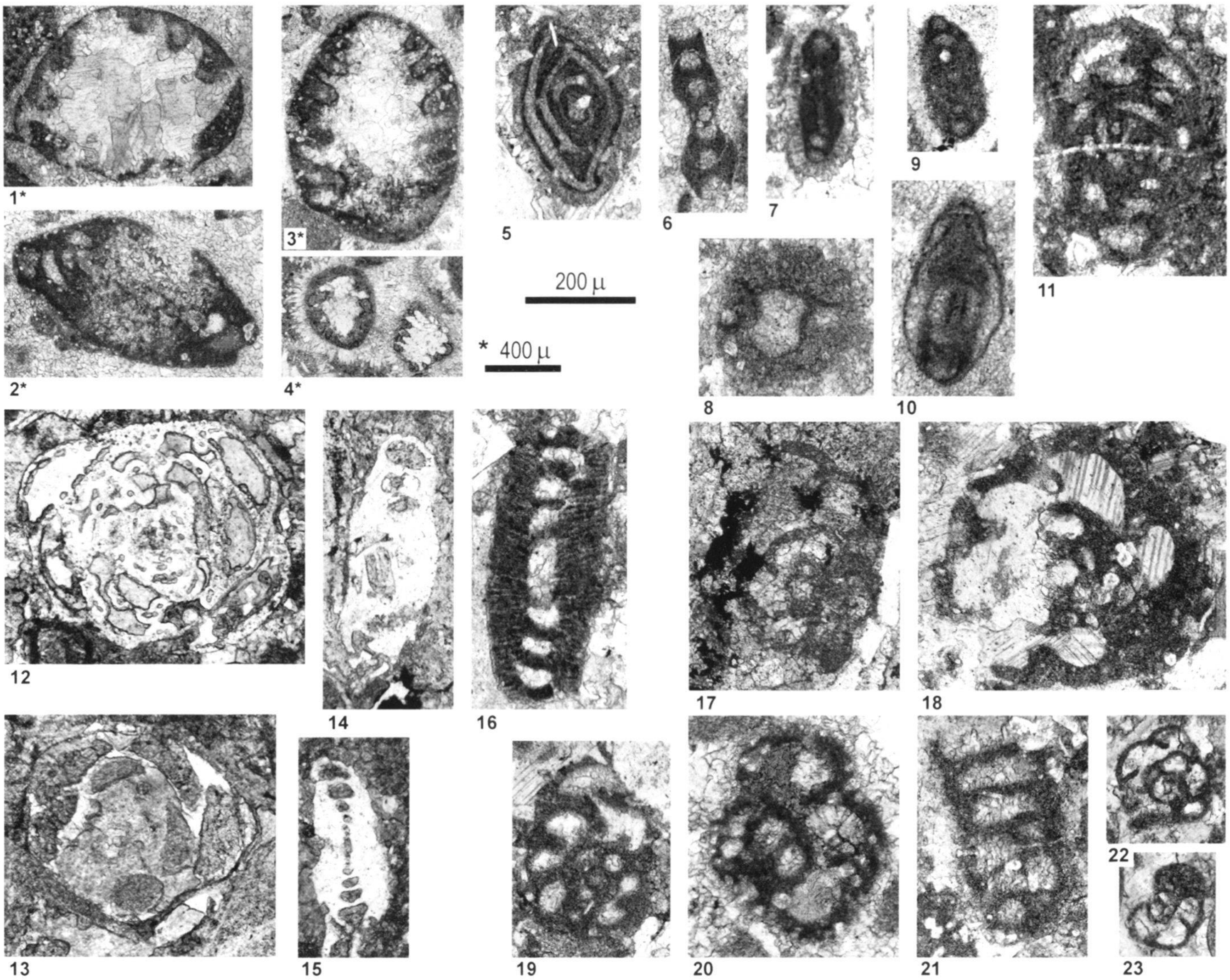

Plate 7

Fig. 1.	*Auloconus permodiscoides* (Oberhauser). Sample H511.
Fig. 2.	*Auloconus sinuosus* Weynschenk. Sample H511.
Fig. 3.–4.	*Auloconus* sp. Samples: H511 (3); H510 (4).
Fig. 5.–7.	*Ophthalmidium sp.* Samples: H5/5 (5); H134 (6); H351 (7).
Fig. 8.	*Cucurbita* sp. Sample H510.
Fig. 9.–10.	*Orthotrinacria sp.* Samples: H5/6 (9); H134 (10).
Fig. 11.	*Pilammina gemerica* Salaj. Sample H5/5.
Fig. 12–13.	*Aulotortus praegaschei* (Koehn-Zaninetti). Sample Mb122.
Fig. 14.–15.	*Triadodiscus eomesozoicus* (Piller). Samples: Mb95 (14); Mb100 (15).
Fig. 16.	*Aulotortus* sp. Sample 127.
Fig. 17.–18., 20.	*Endoteba* aff. *E. controversa* Vachard & Razgallah. Samples: Mb157 (17); H5/5 (18); H511 (20).
Fig. 19.	*Endotebanella* sp. Sample H5/5.
Fig. 21.	*Endotriadella* sp. Sample H5/5.
Fig. 22.–23.	*Endotriada* aff. *E. tyrrhenica* Vachard et al. Sample H5/1

Tab. 1. Conodont data from the Sal section WNW of the village Sal (cf. Fig. 4 and Fig. 5).

No.	*conodonts*	*age*
H 606	– *Neospathodus* cf. *homeri* Bender	Spathian / Late Scythian
98/25	– *Neospathodus symmetricus* Orchard – *Neogondolella jubata* Sweet	Spathian / Late Scythian
98/23	– *Neospathodus* cf. *abruptus* Orchard	Spathian / Late Scythian
H 609	– *Neogondolella* cf. *regalis* Mosher – *Gladigondolella budurovi* Kovacs & Kozur – *Nicoraella kockeli* (Tatge) – *Nicoraella germanica* (Kozur)	Bithynian / Middle Anisian
H 612	– *Neogondolella* cf. *praeszaboi* (Kovacs, Pappsova & Perri)	Late Anisian
0/47	– *Paragondolella excelsa* Mosher – *Paragondolella trammeri* (Kozur) – *Paragondolella liebermanni* (Kovacs & Krystyn) – *Budurovignathus* cf. *hungaricus* (Kozur & Vegh) – *Neogondolella transita* (Kozur)	Upper Fassanian
98/17	– *Paragondolella trammeri* (Kozur) – *Paragondolella inclinata* (Kovacs) – *Budurovignathus hungaricus* (Kozur & Vegh) reworked: – *Gondolella* cf. *slovenica* Ramovs, Permian	Longobardian 1
H 615	– *Paragondolella trammeri* (Kozur) – *Paragondolella inclinata* (Kovacs) – *Budurovignathus mungoensis* (Diebel) – *Budurovignathus japonicus* (Hayashi) reworked: – *Neogondolella transita* Kozur, Middle Triassic – *Paragondolella* cf. *excelsa* Mosher, Middle Triassic	Longobardian 1
98/18	– *Paragondolella inclinata* (Kovacs) – *Budurovignathus mungoensis* (Diebel) reworked: – *Gondolella* cf. *slovenica* Ramovs, Permian	Longobardian 2
H 835	– *Budurovignathus mungoensis* (Diebel) – *Paragondolella inclinata* (Kovacs) – *Gladigondolella tehydis* (Huckriede) + ME reworked: – *Gondolella* cf. *slovenica* Ramovs, Permian – *Neospathodus homeri* (Bender), Spathian – *Neogondolella bulgarica* (Budurov & Stefanov), Anisian – *Nicoraella kockeli* (Tatge), Anisian	Longobardian 2–3
H 836	– *Metapolygnathus polygnathiformis* (Budurov & Stefanov) – *Metapolygnathus foliatus* (Budurov & Stefanov) – *Metapolygnathus carnicus* (Krystyn) – *Paragondolella inclinata* (Budurov & Stefanov) – *Gladigondolella malayensis* (Nogami) + ME reworked: – *Gondolella* cf. *slovenica* Ramovs, Permian	Julian 1/2 boundary
	– *Neospathodus* cf. *dieneri* (Sweet), Dienerian – *Neospathodus homeri* (Bender), Spathian	
98/20 H 834	– *Metapolygnathus foliatus* (Budurov & Stefanov) – *Glandigondella tethydis* (Huckriede) + ME	Julian 1-2
H 842	– *Metapolygnathus polygnathiformis* (Budurov & Stefanov) – *Metapolygnathus foliatus* (Budurov & Stefanov) – *Metapolygnathus auriformis* (Kovacs) – *Gladigondolella malayensis* (Nogami) + ME reworked: – *Gondolella* cf. *slovenica* Ramovs, Permian	Julian 2

No.	conodonts	age
98/21	– *Metapolygnathus foliatus* (Budurov & Stefanov) – *Metapolygnathus polygnathiformis* (Budurov & Stefanov) – *Gladigondolella tethydis* + ME reworked: – *Neospathodus* cf. *dieneri* Sweet, Dienerian – *Neospathodus* cf. *triangularis* Bender, Dinerian	Julian 2
0/45 0/46 H 843	– *Metapolygnathus polygnathiformis* (Budurov & Stefanov) – *Metapolygnathus carpathicus* (Kozur & Mock)	Tuvalian 2
H 833	– *Metapolygnathus polygnathiformis* (Budurov & Stefanov) – *Metapolygnathus nodosus* Hayashi	 Tuvalian 3
H 832	– *Metapolygnathus oertlii* Kozur – *Metapolygnathus communisti* Hayashi	Tuvalian 3
H 831	– *Metapolygnathus communisti* Hayashi – *Metapolygnathus oertlii* Kozur – *Metapolygnathus pseudodiebeli* (Kozur) reworked: – *Gondolella* cf. *slovenica* Ramovs, Permian – *Neospathodus dieneri* Sweet, Dienerian – *Gladigondolella* + ME Anisian to Julian – *Metapolygnathus polygnathiformis* (Budurov & Stefanov), Carnian	Tuvalian 3
H 830	– *Metapolygnathus communisti* Hayashi – *Norigondolella navicula* (Huckriede) – *Epigondolella* sp. reworked: – *Gondolella* cf. *slovenica* Ramovs, Permian – *Neospathodus dieneri* Sweet, Dienerian – *Gladigondolella* + ME Anisian to Julian – *Metapolygnathus polygnathiformis* (Budurov & Stefanov), Carnian – *Metapolygnathus oertlii* Kozur, Tuvalian – *Metapolygnathus pseudodiebeli* (Kozur)	Lacian 1
H 829	– *Metapolygnathus communisti* Hayashi – *Norigondolella navicula* (Huckriede) – *Epigondolella* sp. reworked: – *Gondolella* cf. *slovenica* Ramovs, Permian – *Neospathodus* cf. *homeri* (Bender), Spathian	Lacian 1
H 828	– *Norigondolella navicula* (Huckriede) – *Epigondolella* sp. reworked: – *Metapolygnathus oertlii* Kozur, Tuvalian	Lacian 1
H 616	– *Epigondolella quadrata* Orchard	Lacian 1/II
H 876	– *Misikella posthernsteini* Kozur & Mock – *Misikella hernsteini* Mostler reworked: – *Gondolella* cf. *slovenica* Ramovs, Permian – *Neospathodus dieneri* Sweet, Dienerian – *Epigondolella postera* (Kozur & Mostler), Middle Norian – *Epigondolella quadrata* Orchard, Early Norian	Rhaetian

Tab. 2. Overview of the radiolarian assemblages and their age.

No.	*UTM coord.*	*Radiolarians*	*Age*
H 827	762478/2449654	*Eptingium manfredi* Dumitrica *Pararchaeospongoprunum* cf. *hermi* Lahm *Paroertlispongus multispinosus* Kozur & Mostler	Late Anisian
H 828	762478/2449654	*Bulbocyrtium* sp. *Eptingium manfredi* Dumitrica *Hindeosphaera* sp. *Paronaella (?)* sp. *Plafkerium (?) contortus* Dumitrica, Kozur & Mostler *Pseudoertlispongus mostleri* Kozur *Pseudostylosphaera japonica* (Nakaseko & Nishimura) *Spongopallium hadra* (Sugiyama) *Tetraspinocyrtis* (?) sp. (n. sp.)	uppermost Illyrian -? lowermost Fassanian
A 181	754600/2433550	*Archaeocenosphaera* (?) spp. – common *Baumgartneria trifurcata* Dumitrica *Baumgartneria* n. sp. *Cryptostephanidium* sp. *Falcispongus falciformis* Dumitrica *Oertlispongus* cf. *inaequispinosus* Dumitrica, Kozur & Mostler *Pentactinocarpus* cf. *acanthicus* Dumitrica *Pentaspongodiscus* cf. *anisicus* Kozur & Mostler *Pseudostylosphaera japonica* (Nakaseko & Nishimura) *Turospongus* (?) sp.	Fassanian
P 373	769697/2426212	*Annulotriassocampe campanilis* Kozur & Mostler *Baumgartneriu transita* Dumitrica *Baumgartneria stellata* Dumitrica *Cryptostephanidium cornigerum* Dumitrica *Eptingium manfredi* Dumitrica *Falcispongus calcaneum* Dumitrica *Falcispongus falciformis* Dumitrica *Goestlingella illyrica* Kozur *Oertlispongus longispinosus* Dumitrica, Kozur & Mostler *Pararuesticyrtium fusiformis* (Bragin) *Paroertlispongus multispinosus* Kozur & Mostler *Pentactinocarpus fusiformis* Dumitrica *Planispinocyrtis baloghi* Kozur & Mostler *Pseudostylosphaera japonica* (Nakaseko & Nishimura) *Spongopallium contortum* Dumitrica, Kozur & Mostler *Spongopallium hadra* (Sugiyama) *Spongosilicarmiger italicus* Kozur & Mostler *Tiborella* cf. *magnidentata* Dumitrica, Kozur & Mostler *Triassocampe nodosoannulata* (Kozur & Mostler) *Triassocampe scalaris* Dumitrica, Kozur & Mostler	Early-Middle Fassanian
A 121	772282/2475593	*Archaeocenosphaera* (?) spp. *Baumgartneria retrospina* Dumitrica *Eptingium manfredi* Dumitrica *Oertlispongus inaequispinosus* Dumitrica, Kozur & Mostler *Pseudostylosphaera* sp.	Fassanian
H 508	777672/2455271	*Archaeocenosphaera* sp. *Eptingium manfredi* Dumitrica *Oertlispongus inaequispinosus* Dumitrica, Kozur & Mostler *Pseudostylosphaera* sp.	Fassanian
A 119	772194/2474998	*Archaeocenosphaera* (?) spp. *Falcispongus hamatus* Dumitrica *Parasepsagon* (?) sp. *Paroertlispongus multispinosus* Kozur & Mostler *Pseudostylosphaera canaliculata* (Bragin) *Pseudostylosphaera* sp. B of Yeh 1992 *Sepsagon* (?) *robustus* Lahm *Silicarmiger latus* Kozur & Mostler *Striatotriassocampe* cf. *laeviannulata* Kozur & Mostler	Early Longobardian

No.	*UTM coord.*	*Radiolarians*	*Age*
A 122	772282/2475593	*Archaeocenosphaera* (?) spp.	Longobardian?
		Eptingium (?) sp.	
		Muelleritortis (?) aff. *cochleata* (Nakaseko & Nishimura)	
H 429	783577/2475792	*Archaeocenosphaera* (?) spp.	Middle-Late Longobardian
		Triassocampe (?) spp.	
		Muelleritortis cochleata (Nakaseko & Nishimura)	
		Pseudostylosphaera sp.	
P 378	767950/2428858	*Archaeosemantis pterostephanus* Dumitrica	uppermost Longobardian
		Bogdanella cf. *trentana* Kolar-Jurkovsek	lowermost Cordevolian
		Corum (?) sp.	
		Dumitricasphaera sp.	
		Hsuum (?) aff. *cordevolicum* Kozur & Mostler	
		Muelleritortis koeveskalenensis Kozur	
		Ornatisaturnalis translatus Mostler & Krainer	
		Spongoserrula rarauana Dumitrica	
		Spongostylus tortilis Kozur & Mostler	
		Triassocampe (?) sp.	
		Triassostephanidium anisicum Kozur, Krainer & Mostler	
		Tritortis dispiralis (Bragin)	
		Tritortis kretaensis (Kozur & Krahl)	
		Vinassaspongus subsphaericus Kozur & Mostler	
		Xiphotheca (?) *dimidiata* Bragin	
A 137	761156/2444708	*Tritoritis kretaensis* (Kozur &Krahl)	uppermost Longobardian
		Muelleritortis cochleata (Nakaseko & Nishimura)	lowermost Cordevolian
		Eptingium manfredi Dumitrica	
		Pseudostylosphaera sp.	
A 107	763233/2427123	*Tritortis kretaensis* (Kozur & Krahl)	Early Carnian
		Baumgartneria stellata Dumitrica	
		Spongoserrula rarauana Dumitrica	
		Divatella (?) sp.	
		Capnuchosphaera sp.	
H 512	777672/2455271	*Pseudostylosphaera* sp.	Early Carnian
H 844	783547/2474428	*Archaeocenosphaera* sp.	Middle-Late Carnian
		Capnodoce (?) sp. cf. *venusta* Pessagno	
		Capnuchosphaera colemani Blome	
		Capnuchosphaera crassa Yeh	
		Capnuchosphaera deweveri Kozur & Mostler	
		Capnuchosphaera cf. *lea* De Wever	
		Capnuchosphaera silviensis Blome	
		Capnuchosphaera tortuosa Yeh	
		Kahlerosphaera philippinensis Yeh	
		Kahlerosphaera sp.	
		Latium mumdum Blome	
		Paronaella (?) sp.	
		Poulpus pansus De Wever	
		Pseudostylosphaera (?) sp.	
		Spongostylus carnicus Kozur & Mostler	
		Trialatus cf. *megacornutus* Yeh	
		Triassocampe sulovensis Kozur & Mock	
		Xiphotheca karpenissionensis De Wever	
		Zhamoidasphaera cf. *proceruspinosa* Lahm	
A 198	774174/2436830	*Archaeocenosphaera* (?) spp.	Late Carnian-Early Norian
		Canesium (?) sp.	
		Canoptum sp. A of Blome 1984	
		Capnuchosphaera crassa Yeh	
		Capnuchosphaera colemani Blome	
		Capnuchosphaera palawaensis Yeh	
		Capnuchosphaera cf. *soldierensis* Blome	
		Capnuchosphaera cf. *theloides* De Wever	
		Pachus (?) sp.	
		Poulpus piabyx De Wever	

No.	*UTM coord.*	*Radiolarians*	*Age*
		Sarla cf. *vizcainoensis* Pessagno *Sarla* sp. *Spongostylus* cf. *carnicus* Kozur & Mostler *Trialatus* sp.	
A 56	768750/2446515	*Archaeocenosphaera* sp. *Capnuchosphaera deweveri* Kozur & Mostler *Capnuchosphaera triassica* De Wever *Capnuchosphaera theloides* De Wever *Capnuchosphaera lea* De Wever *Capnuchosphaera palawanensis* Yeh *Divatella spinosa* Kozur & Mostler *Kahlerosphaera longispinosa* Kozur & Mostler *Kahlerosphaera philipinensis* Yeh *Paronaella* sp. – very rare *Praeheliostaurus levis* Kozur & Mostler *Spongostylus carnicus* Kozur & Mostler *Spongostylus tortilis* Kozur & Mostler *Trialatus* cf. *megacornutus* Yeh	Middle – Late Carnian
H 621	783547/2474428	*Archaeocenosphaera* (?) spp. *Capnodoce anapetes* De Wever *Capnuchosphaera triassica* De Wever *Capnuchosphaera colemani* Blome *Capnuchosphaera* sp. *Canoptum* spp. *Castrum perornatum* Blome *Castrum* (?) sp. *Corum regium* Blome *Latium mundum* Blome *Latium paucum* Blome *Syringocapsa* sp.	Early-Middle Norian
A 125	783722/2475604	*Canesium (?) cf. cucurbita* Sugiyama *Canoptum* sp. *Capnodoce* cf. *anapetes* De Wever *Capnodoce* cf. *antiqua* Blome *Capnuchosphaera lea* De Wever *Capnuchosphaera puncta* De Wever *Capnuchosphaera* cf. *silviesensis* Blome *Capnuchosphaera* cf. *theloides* De Wever *Capnuchosphaera tricornis* De Wever *Latium mundum* Blome *Spongostylus* cf. *carnicus* Kozur & Mostler *Triassocampe* sp. *Xiphoteca rugosa* Bragin	Early Norian

Tab. 3. Foraminifers data from the Sal Formation.

No.	*UTM coord.*	*Foraminifers*	*Ages*
H351		*Ophthalmidium* sp. Endotebidae	
H566		*Turriglomina mesotriasica* (Koehn-Zaninetti)	Middle Ladinian
H614		*Turriglomina mesotriasica* (Koehn-Zaninetti) *Gsollbergella spiroloculiformis* (Oravecz-Scheffer) *Lenticulina* spp.	
Mb95		*Turriglomina* aff. *T. magna* (Urosevic) *Turriglomina conica* (He Yan) *Turriglomina* aff. *T. scandonei* Zaninetti et al. *Aulotortus sinuosus* Weynschenk *Endotriada* sp. *Lenticulina* spp.	Middle Ladinian to Middle Carnian
Mb100	762478/2449654	*Palaeolituonella meridionalis* (Luperto) *Triadodiscus eomesozoicus* (Piller)	
Mb122		*Aulotortus praegachei* (Koehn-Zaninetti) *Lenticulina* spp.	
Mb151		*Duotaxis* sp. *Lenticulina* spp. Endotebidae	
Mb157		*Endoteba* aff. *E. controversa* Vachard & Razgallah	Carnian to Early-Middle Norian
Mb182		*Turriglomina* aff. *T. magna* (Urosevic) *Lenticulina* spp.	
Mb127		*Aulotortus* sp. *Duotaxis* sp. *Endoteba* sp. *Lenticulina* spp.	
H510		*Auloconus* sp.	
H510/I		*Cucurbita* sp.	
H511		*Aulotortus sinuosus* Weynschenk *Auloconus permodiscoides* (Oberhauser) *Auloconus* sp. *Turriglomina* aff. *T. magna* (Urosevic) *Endoteba* aff. *E. controversa* Vachard & Razgallah	
H5/1	777672/2455271	*Endotriada* aff. *E. tyrrhenica* Vachard et al. *Glomospira* sp. Duostominidae	Early Ladinian to Early Carnian
H5/5		*Pilammina gemerica* Salaj *Ophthalmidium* sp. *Endotriada* sp. *Endotriadella* sp.	
H5/6		*Orthotrinacria* sp. *Endotriada* sp.	
H5/7		*Turriglomina mesotriasica* (Koehn-Zaninetti)	
H5/10		*Palaeolituonella meridionalis* (Luperto)	
H99	770947/2449079	*Planinvoluta* sp.	
H134	766323/2441950	*Planinvoluta carinata* Leischner *Cucurbita* sp. *Ophthalmidium* sp. *Orthotrinacria* sp. Duostominidae	Middle to Late Triassic

Tab. 4. Whole rock carbon and oxygen isotope results from the Sal section.

Sample No.	distance	$\delta^{13}C$	$\delta^{18}O$
Mb 2	2	1.13	-4.78
Mb 5	5	0.15	-5.09
Mb7	7	1.1	-4.97
Mb 10	10	1.84	-4.52
Mb 13	13	2.95	-5.13
Mb 16	16	7	-4.88
Mb 24	24	4.5	-5.08
Mb 27	27	2.6	-4.42
Mb 37	37	-2.57	-8.46
Mb 40	40	-2.36	-8.79
Mb 46	46	-1.8	-5.61
Mb 50	50	1.68	-3.19
Mb 56	56	1.34	-3.65
Mb 64	64	0.38	-5.22
Mb 65	65	-1.64	-6.44
Mb 66	66	-0.24	-6.96
Mb 69	69	-0.95	-9.61
Mb 73	73	-1.39	-7.32
Mb 75	75	0.43	-6.67
Mb 78	78	-0.09	-9.45
(Mb 78a)	78	0.85	-5.7
Mb 81	81	0.46	-6.87
Mb 82	82	-0.98	-5.13
H 835	85	-0.21	-7.12
Mb 95	95	0.5	-7.83
I 99.5	99.5	1.41	-5.5
Mb 100	100	0.08	-5.64
Mb 103	103	-0.6	-4.87
I 104	104	0.56	-3.75
Mb 105	105	1.76	-3.13
Mb 108	108	2.7	-2.42
Mb 110	110	1.31	-5.32
H 842	121	1.66	-2.73
Mb122	122	-0.21	-6.65
I 127	127	0.82	-7.45
I 131	131	0.07	-3.61
H 843	134	0.2	-4.85
H 832	145	-0.06	-8.2
Mb 151	151	1.1	-5.55
H 831	155	1.13	-5.73
Mb 157	157	1 -	4.09
Mb 159	159	1.18	-7
H 830	162	1.2	-7.31
H 829	166	0.29	-5.87
Mb 169	169	1.1	-8.77
H 828	171	1.48	-1.96
Mb 172	172	1.67	-7.3
Mb 175	175	1.52	-5.99
H 844	179	1.36	-5.9
Mb 180	180	0.92	-6.04
Mb127	182	0.58	-9.17
Mb 182	182	-0.39	-7.86